

Alma Mater Studiorum - Università di Bologna

DOTTORATO DI RICERCA IN
SCIENZE BIOMEDICHE E NEUROMOTORIE

Ciclo 35

Settore Concorsuale: 06/D6 - NEUROLOGIA

Settore Scientifico Disciplinare: MED/26 - NEUROLOGIA

SKIN AS A PROMISING BIOMATRIX FOR THE EARLY DETECTION OF
MISFOLDED PROTEINS BY RT-QUIC IN NEURODEGENERATIVE DISEASES

Presentata da: Angela Mammana

Coordinatore Dottorato

Matilde Yung Follo

Supervisore

Piero Parchi

Esame finale anno 2023

ABSTRACT

Real-Time Quaking-Induced Conversion (RT-QuIC) is an ultrasensitive assay capable of detecting pathological aggregates of misfolded proteins in biospecimens. In recent years, efforts have been made to find a more feasible and convenient biomatrix as an alternative to CSF, and skin biopsy may be a suitable candidate. This project aimed to evaluate the diagnostic performance of skin RT-QuIC in 3 different cohorts of patients: 1. Creutzfeldt-Jakob disease (CJD), 2. Lewy body disease (LBD), and 3. Isolated REM sleep behavior disorder (iRBD).

We studied 71 punch skin samples of 35 patients with CJD, including five assessed in *vitam*, using 2 different substrates: *Bank vole* 23-230 (Bv23-230) and *Syrian hamster* 23-231 (Ha23-231) recombinant prion protein. Skin prion RT-QuIC showed a 100% specificity with both substrates and a higher sensitivity with the Bv23-230 than Ha23-231 (87.5% vs. 65.6%, respectively). Forty-one patients underwent both lumbar puncture (LB) and skin biopsy; CSF and skin RT-QuIC showed a high level of concordance (38/41, 92.7%).

Then, we analyzed samples taken in *vitam* (n=69) or postmortem (n=49) from patients with Parkinson's disease (PD), dementia with Lewy bodies (DLB), incidental Lewy body pathology, and neurological controls. Skin α -syn RT-QuIC distinguished LBD patients with an overall accuracy of 94.1% in the two cohorts (sensitivity, 89.2%; specificity, 96.3%). Seventy-nine patients underwent both CSF and skin α -syn RT-QuIC, and the two assays yielded similar diagnostic accuracy (skin, 97.5%; CSF, 98.7%).

Finally, we studied 91 iRBD patients and 41 control. In the skin, RT-QuIC showed a sensitivity of 76.9%, specificity of 97.6%, and 82.0% accuracy. 128 participants (88 patients plus 40 controls) underwent both CSF and skin RT-QuIC. The two protocols showed 99.2% of concordance.

These works confirmed that skin punch biopsies might represent a valid and convenient alternative to CSF analysis for an early diagnosis of prion diseases and LB-related pathologies.

INDEX

INTRODUCTION	1
Neurodegenerative diseases	1
Prion diseases	1
Cellular prion protein	2
PrP scrapie	3
Human prion diseases	4
Mutations and polymorphisms in PRNP	5
PrP ^{Sc} types and the molecular basis of sCJD heterogeneity	6
PrP ^{Sc} cellular and tissue spread	8
Synucleinopathies	9
Synuclein protein family	9
α -synuclein	10
Synucleinopathies and alpha-synuclein strains	11
Parkinsons's disease	13
Dementia with Lewy Body	13
REM sleep behavior disorder	14
Alpha-synuclein cellular and tissue spread	14
Real-Time Quaking-Induced Conversion (RT-QuIC) assay	15
A brief history	15
The need for new early biomarkers for neurodegenerative diseases	17
RT-QuIC assay across prion diseases	18
RT-QuIC assay across synucleinopathies	18
RT-QuIC biomatrices across prion diseases and synucleinopathies	19
Ph.D. RESEARCH PROJECT	21
MATERIALS AND METHODS	22
<i>Mammana, Angela et al. "Detection of prions in skin punch biopsies of Creutzfeldt-Jakob disease patients."</i>	22
CJD patients and controls	22
Neuropathological examination	23
CSF collection and analyses	24
Skin biopsy procedure and sample preparation	24
Prion RT-QuIC	25
Statistical analysis	26
<i>Mammana, Angela, et al. "RT-QuIC Detection of Pathological α-Synuclein in Skin Punches of Patients with Lewy Body Disease."</i>	26

LBD patients and controls	26
Skin biopsy procedure and sample preparation	27
α -Syn RT-QuIC	27
Statistical analysis	28
<i>Alex Iranzo, Angela Mammana, et al. "Misfolded α-synuclein assessment in skin and CSF by RT-QuIC in isolated REM sleep behaviour disorder"</i>	28
iRBD patients and controls	28
Skin biopsy procedure and sample preparation	30
α -Syn RT-QuIC	31
Statistical analysis	31
RESULTS	33
<i>Mammana, Angela et al. "Detection of prions in skin punch biopsies of Creutzfeldt-Jakob disease patients."</i>	33
Sample preparation and optimization of experimental conditions for skin prion RT-QuIC	33
RT-QuIC assay: comparison between Ha23-231 and Bv23-230 recombinant prion protein	33
Comparison of prion seeding activity detection in skin and CSF samples from the same patient	35
RT-QuIC detection of prion in skin punch biopsies taken in vivo	36
<i>Mammana, Angela et al. "RT-QuIC Detection of Pathological α-Synuclein in Skin Punches of Patients with Lewy Body Disease"</i>	38
Optimization of experimental conditions for skin α -Syn RT-QuIC	38
RT-QuIC analysis of post-mortem skin punches for the detection of synuclein seeding activity	39
Comparison of α -Synuclein seeding activity detection in skin and CSF samples from the same patient	44
<i>Alex Iranzo, Angela Mammana, et al. "Misfolded α-synuclein assessment in skin and CSF by RT-QuIC in isolated REM sleep behaviour disorder"</i>	44
RT-QuIC analysis of skin biopsies for the detection of synuclein seeding activity in iRBD patients	44
Comparison of α -Synuclein seeding activity detection in skin and CSF samples from the same patient	46
DISCUSSION AND CONCLUSIONS	49
BIBLIOGRAPHY	53

SKIN AS A PROMISING BIOMATRIX FOR THE EARLY DETECTION OF MISFOLDED PROTEINS BY RT-QUIC IN NEURODEGENERATIVE DISEASES

INTRODUCTION

Neurodegenerative diseases

Neurodegenerative diseases constitute a significant health problem for the world's aging population. They are currently classified among organ-specific amyloidosis and include Alzheimer's disease, α -synucleinopathies, tauopathies, prion diseases, and transactivation response DNA binding protein43 (TDP-43)-pathies.¹ Proteins involved in neurodegenerative diseases show a common abnormal conformation characterized by a beta sheet-rich secondary structure. These misfolded proteins are prone to aggregate and organize themselves into filamentous aggregates, mostly found within the cytoplasm of neurons and glia. Although different protein accumulation and preferential vulnerability define these pathologies, they share many important processes associated with neuronal dysfunction and death. They include proteotoxic stress leading to abnormalities in ubiquitin-proteasomal and autophagosomal/lysosomal systems, neuroinflammation, and oxidative stress.¹ The current diagnostic gold standard for neurodegenerative diseases is a neuropathological evaluation at autopsy investigating the presence, morphology, and distribution of aggregates by immunohistochemistry.¹

Prion diseases

Prion diseases or transmissible spongiform encephalopathies (TSEs) are a group of rapid and fatal neurodegenerative diseases affecting both humans and animals. Scrapie was the first described prion disease, and its transmissible nature was discovered following experimental inoculation of brain homogenate from a scrapie-infected sheep to a healthy sheep.² In 1920, Hans Gerhard Creutzfeldt e Alfons Maria Jakob described the first TSE in humans, which was named, Creutzfeldt-Jakob disease (CJD) after them.^{3,4} Given the infectious nature of TSEs, many attempts were made to understand the fundamental nature of the agent causing these diseases. In 1982, Stanley Prusiner first coined the term "prion," PRoteinaceous Infectious Only Particles, based on the hypothesis that a protein is the only component of the agent causing transmissible spongiform encephalopathies.⁵ Subsequent studies by Prusiner and Bolton on homogenates of infected hamster brains led to the identification of a pathological misfolded form of the prion protein, PrP^{Sc}, as the putative etiologic agent of TSEs⁶ and in 1986, Oesch and Basler first identified the putative gene encoding the prion protein.⁷

Cellular prion protein

PRNP is a single-copy gene localized on the short arm of chromosome 20; it is made by two exons, the last of which encodes for the 253 aminoacidic prion protein. PrP^C (where C means cellular) comprises a flexible unstructured N-terminal tail, containing a nonapeptide followed by 4 repetitions of an octapeptide sequence, a central globular domain with three alpha-helices and two antiparallel β -sheet and a C-terminal tail.^{8,9} After synthesis, prion protein undergoes a post-translation modification process, which involves the removal of a peptide from the N-terminal, the addition of a glycosylphosphatidylinositol (GPI) anchor at the C terminus,¹⁰ and the attachment of complex oligosaccharides chains at the two-asparagine residue in position 181 and 197. The latter generates three differently glycosylated forms of prion protein: diglycosylated, monoglycosylated, and unglycosylated.¹¹ In its mature form, PrP^C is present mainly as a diglycosylated protein, localized at the outer side of the plasma membrane in lipid-enriched microdomains (Figure 1).¹²

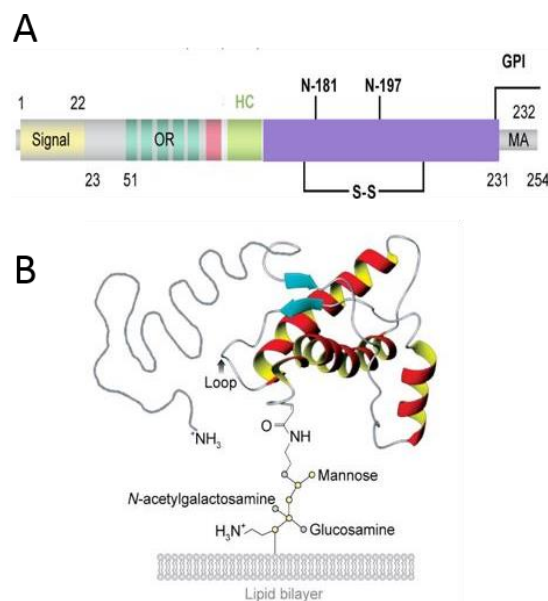


Figure 1. Structural features and biochemical properties of the cellular prion protein. A) Schematic diagram of the primary structure of PrP. The protein consists of three domains: an N-terminal domain (51-91), a globular domain (125-228), and a flexible C-terminal domain (229-231). Post-translational modifications are shown: oligosaccharides bound to asparagine residues 181 and 197 and the GPI anchor. B) Tertiary structure of the cellular prion protein, as deduced from NMR spectroscopy, inserted into a lipid bilayer, including the unstructured N-terminal tail (gray) and the GPI anchor. Sugar residues are shown as colored small circles. Figure adapted from Aguzzi et al., *Annu Rev Pathol.* 2008.¹³

Following internalization, PrP^C can either be recycled to the plasma membrane or the Golgi (retromer pathway)¹⁴ or is transported to late endosomes. It could also reside in the plucked-off

intraluminal vesicles within multivesicular bodies (MVBs) for release as exosomes or degradation in lysosomes.^{15,16}

The putative roles of the protein, expressed mainly in the central nervous system (CNS) but also in lymphoid, spleen, skin, and muscles, are neuroprotection, oxidative stress reduction,¹⁷ cellular adhesion,¹⁸ and synaptic plasticity.¹⁹

PrP scrapie

The disease-specific conformation of PrP is denoted as PrP^{Sc} (where Sc stands for the pathogenic version of the protein found in sheep suffering from “scrapie”), which shares the same primary amino acid sequence with the cellular counterpart, but differs drastically in protein conformation, resulting in distinct properties. Specifically, PrP^C is highly α -helical, soluble in mild detergents, and sensitive to protease digestion. In contrast, PrP^{Sc} is mainly β -sheet, highly aggregated, and partially resistant to PK (proteinase-K) digestion (Figure 2).

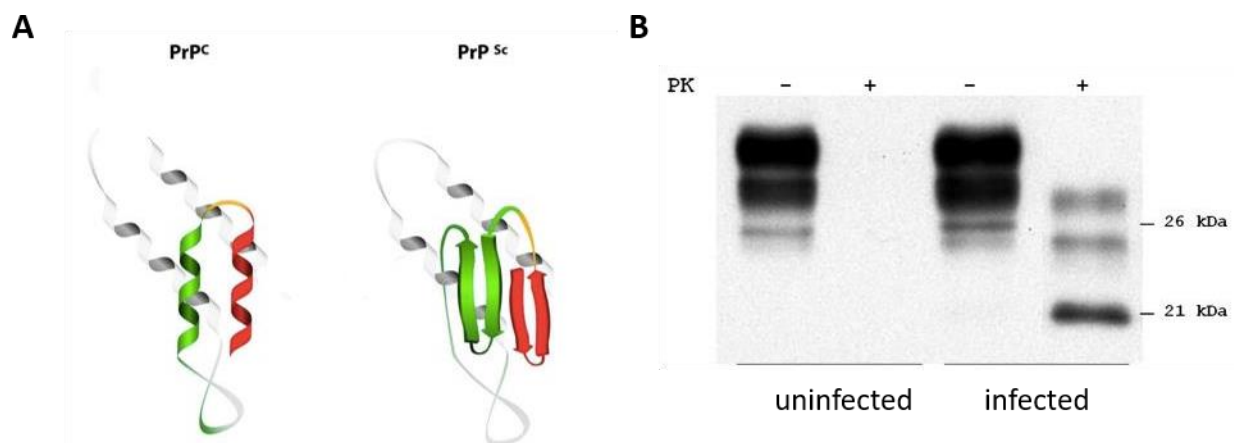


Figure 2. Comparison of structure and biochemical properties of PrP^C and PrP^{Sc}. A) The figure shows the structure of the cellular prion protein and the pathological form highlighting the structural changes and in particular the transition from a structure predominantly alpha helix to the the high beta-sheet content of PrP^{Sc}. B) Western blot showing the pattern of glycosylation of PrP^C and PrP^{Sc}. In the absence of PK, the two proteins show the same glycosylation profile, whereas when the protein is subjected to PK treatment, PrP^{Sc} shows resistance, while the physiological form is completely digested.

The mechanism underlying the conversion of PrP^C to PrP^{Sc} remains unknown. It was hypothesized that after PrP^C translation, some external factors like oxidative stress, age, or inflammatory response might cause its misfolding. At this point, some molecular chaperons, named heat shock protein (Hsp), act by helping protein refolding or degradation through the ubiquitin-proteasome quality

control (UPS).²⁰ However, other HSPs may stabilize this misfolded structure leading to the formation of protein aggregates.

The proposed mechanism for PrP^{Sc} aggregates formation is based on a nucleation and fragmentation process during which highly ordered PrP^{Sc} oligomers, called propagons, can incorporate PrP^C and grow in size arising in the larger structures of fibril and protofibrils.²¹ Fragmentation of these structures creates new propagons, which can restart the cycle by incorporating new protein monomers.²²

Evidence indicates that the conversion process might take place on the plasma membrane or in the endocytic pathway, within multivesicular bodies (MVBs), as preventing MVB maturation reduce PrP^{Sc} production.¹⁵

The mechanisms of the pathophysiology of prion diseases are still an open question; it is conceivable that both the partial loss of some physiological functions of PrP^C and the presence of PrP^{Sc} aggregates may contribute directly or indirectly to prion-associated neurodegeneration.

PrP^{Sc} aggregates might act in the intracellular compartment disrupting protein homeostasis and blocking the unfolded protein response (UPR) pathways²³⁻²⁵ or causing neuronal membrane injury corrupting the function of neuronal receptors such as the NMDA receptor.²⁶

Human prion diseases

Prion diseases are a group of neurodegenerative diseases caused by the accumulation and spread of PrP^{Sc} in the central nervous system. Human TSEs are classified into three groups according to their etiology: acquired, caused by the exogenous transmission of PrP^{Sc}; idiopathic, particularly sporadic CJD (sCJD), which accounts for more than 80% of all cases and has an incidence of about 1.5 cases per million; and Inherited, related to mutations in *PRNP*.²⁷

Regardless of etiology and species, prion diseases share specific histopathological features that distinguish them from other neurodegenerative diseases: spongiform change and accumulation of PrP^{Sc} aggregates on the cell membrane (Figure 3), sometimes forming mature extracellular amyloid plaques. Spongiform change consists of vacuoles that are diffuse or clustered and variably found in the neuropil of the cerebral cortex, cerebellar cortex, hippocampus, amygdala, basal ganglia, thalamus, and brainstem.²⁸ Variable degrees of spongiform change and regional distribution and different plaque morphology characterize the different prion diseases.

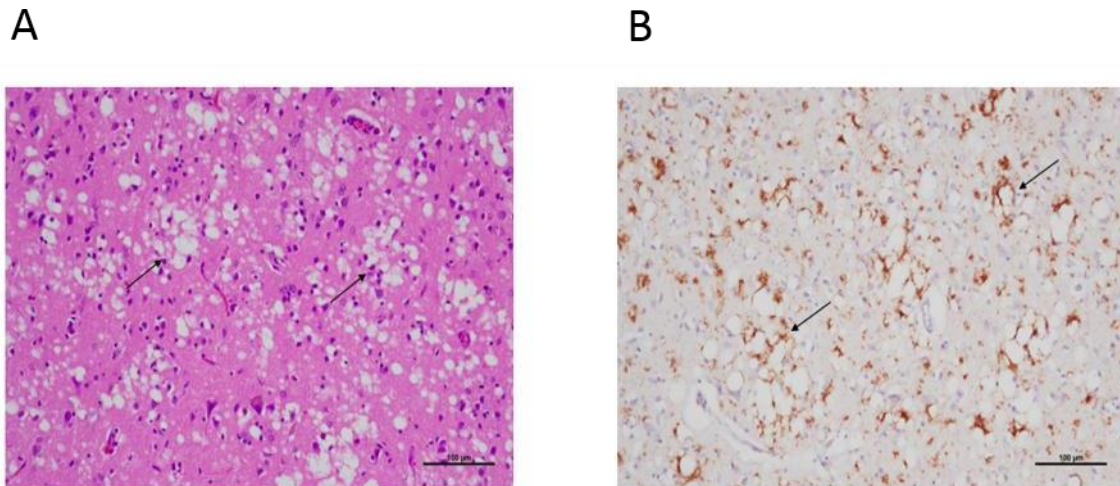


Figure 3. Anatomopathological features of prion diseases. A) Hematoxylin-eosin staining showing the presence of vacuoles, indicated by arrows and spongiosis, associated with massive neuronal loss. Scale bar: 100 µm. B) Perivacuolar PrP^{Sc} deposits. Scale bar: 100 µm. 3F4 antibody.

Mutations and polymorphisms in PRNP

Sequencing of the *PRNP* gene led to the discovery of both mutations, linked to the genetic form of prion diseases, and polymorphisms, including the methionine/valine polymorphism at codon 129, which is essential for disease susceptibility and phenotypic expression.²⁹ In the healthy population, 37% were MM, 51% were MV, and 12% were VV. In contrast, among sCJD cases, 71.6% were MM, 11.7% were MV, and 16.7% were VV.²⁷ Additionally, other polymorphisms of *PRNP* have been described, but it seems that they are silent with no recognizable influence on disease susceptibility or phenotype. These polymorphisms are not determinant either for the sporadic or the genetic form.^{30,31} About 10–15% of subjects who develop a genetic prion disease carry either a point mutation or an insertion of octapeptide repeats (OPR) in the *PRNP* and often have a family history consistent with an autosomal dominant inheritance of variable penetrance disease.³² While most *PRNP* mutations are rare, a few, like E200K and D178N, have been reported worldwide. Indeed, geographical or ethnic clusters of these mutations have been found in Israel, Chile, Italy, and Spain.^{33–36}

Almost all gCJD-associated *PRNP* mutations are located within the protein's globular region, suggesting a role in determining misfolding. Although this is the most plausible theory, few mutations generate changes in protein structure, suggesting that their role could be different from that hypothesized. Indeed, increasing evidence shows that gCJD largely reproduces the phenotypic spectrum of the sCJD variants and that, in both disease forms, the physicochemical properties of PrP^{Sc} and the 129-codon genotype act as major determinants of the disease phenotype. On the

genetic side, it is becoming increasingly clear that mutations per se are not always sufficient to cause the disease and that other environmental or genetic factors also trigger the disease onset.^{32,37}

PrP^{Sc} types and the molecular basis of sCJD heterogeneity

One of the fascinating aspects of prion diseases is phenotypic heterogeneity. Although all symptoms can be linked to neuronal dysfunction and degeneration, they manifest in different ways ranging from cognitive impairment to visual disturbances, from abnormal movements to insomnia.³⁸ Moreover, different diseases show different onset times, clinical courses, and distributions of PrP^{Sc} aggregates in the brain. The basis of this heterogeneity has been well studied in sCJD, the most common human prion disease. In 1999, Parchi and colleagues showed that sCJD comprises 6 different clinical and histopathological subtypes.³⁹ These subtypes are largely determined by the genotype at the polymorphic codon 129 (see the previous paragraph) and by the PrP^{Sc} type. Specifically, based on the electrophoretic mobility of the fragments of PrP^{Sc} obtained after proteinase K (PK) digestion, Parchi et al. originally distinguished two major human PrP^{Sc} types. PrP^{Sc} type 1 has a relative electrophoretic mobility of the unglycosylated form of 21 kDa and a primary cleavage site at residue 82, and PrP^{Sc} type 2 has a relative molecular mass of 19 kDa and a primary cleavage site at residue 97.^{40,41}

Interestingly, PrP^{Sc} types 1 and 2 characterize all subtypes of CJD, regardless of the apparent etiology of the disease (sporadic, inherited, or acquired by infection),^{40,42} suggesting a common mechanism of PrP^{Sc} formation. The results obtained in a large case series demonstrated an overall prevalence of PrP^{Sc} types 1 and 2 co-occurrence of 35%.⁴³ The higher frequency of co-occurrence in MM subjects over the MV and VV indicates that the deposition of type 1 or 2 is not random and is characterized by the coexistence of symptoms related to phenotypic features of the individual subtypes. Most cases with a mixed phenotype were also characterized by clearly identifiable distinctive histopathological traits indicative of the coexistence of two CJD variants within the same brain.⁴³

PrP^{Sc} type prevalence is closely related to the genotype of codon 129, and several studies showed that certain subtypes are related to one genotype rather than others. Specifically, PrP^{Sc} type 1 and the type 1 and 2 co-occurrence are mainly associated with the MM genotype, while type 2 is linked to VV. However, there also are rarer subtypes in which type 1 is associated with the VV genotype and type 2 with MM. In addition to the fragment mentioned above, the analysis of PK-resistant PrP^{Sc}

using C-terminal antibodies showed the presence of other fragments that are specifically associated with some subtypes of CJD (i.e. the 8 kDa fragment associated with the GSS or VPSP).^{44,45}

All this evidence led to the concept of “prion strain,” underlying the heterogeneity of CJD in which the association between PrP^{Sc} type and the genotype of codon 129, led to the existence of 6 different CJD subtypes, MM/MV1, VV2, MV2K, MM/MV2 c, MM2T, VV1 (Figure 4) characterized by specific histopathological features and clinical signs, as shown in Table 1.²⁷

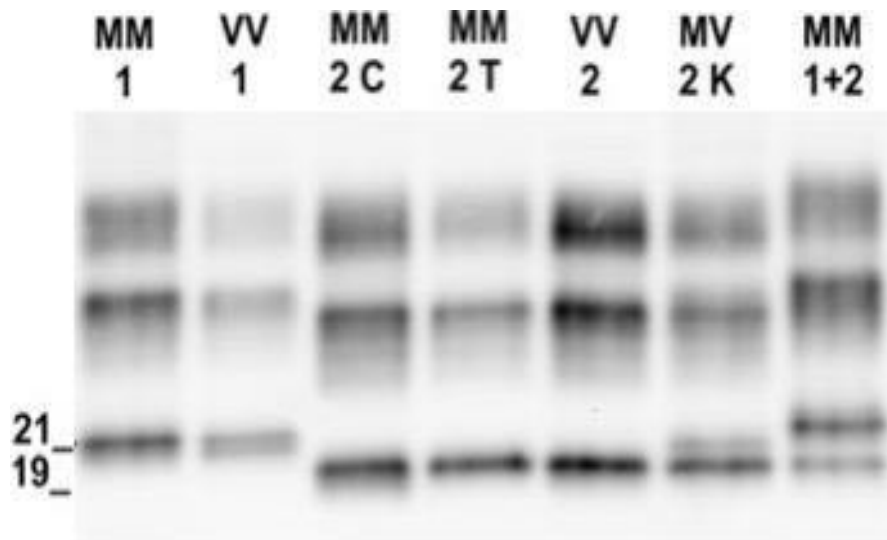


Figure 4. PrP^{Sc} degradation profile. The figure shows the degradation profile of PrP^{Sc} after digestion with protease K of the 6 different subtypes of sCJD. The co-presence of type 1+2 is shown in the last lane. Antibody 3F4.²⁸

Table 1. Nomenclature and distinctive phenotypic features of the sporadic human prion disease (sub)types.

Molecular type	Histopathological type	Clinical features	Age at onset (years)	Disease duration (months)
MM/MV1	Diffuse synaptic deposits	Prominent rapidly progressive dementia. Ataxia is present at onset in 50% of cases and visual impairment in 30%	70.1 (48–86)	4 (1–24)
VV2	Perineuronal and cerebellar plaque-like deposits	Ataxia is often noted at the onset, with dementia supervening in later stages	64.5 (45–83)	6.3 (3–18)
MV 2K	Kuru plaques	Ataxia and dementia are prominent	65.4 (48–81)	15.8 (5–48)
MM/MV 2C	Cortical with confluent vacuoles	Cognitive impairment, myoclonus and pyramidal signs	67.8 (61–75)	20 (12–36)
MM 2T	Thalamo-olivary atrophy	Insomnia and psychomotor hyperactivity are present in most cases. In addition, ataxia and other motor signs are noted	52.3 (36–71)	15.5 (8–24)
VV1	Cortico-striatal synaptic deposits	Progressive dementia with subsequent myoclonus and pyramidal signs	39.3 (24–49)	15.3 (14–16)

Table adopted from Parchi P et al., Acta Neuropathol. 2011.²⁷

PrPSc cellular and tissue spread

The mechanism of the prion spread within the CNS is still poorly understood. It is known that astrocytes are highly susceptible to prion infection in vitro and can readily transfer prions to neurons,^{46,47} while microglia do not play a major role in replication but are instead critical for prion clearance.⁴⁸ In contrast, oligodendrocytes lack any known significant contribution to prion replication or spread through the CNS.⁴⁹ Although much is known about the cells that replicate prions in the brain, little is known about how protein aggregates spread through the brain, from neuron-to-neuron,^{50–52} and between neurons and astrocytes.⁵³ Different studies have proposed different mechanisms: prions may spread cell-to-cell via (i) exosomes^{54,55} and (ii) tunneling nanotubes,^{51,55} with other possible mechanisms yet to be verified, including synaptosomes, GPI-painting, microvesicles, or PrP^{Sc} cleavage from the plasma membrane.⁵⁵

Like some neurotropic infectious agents, prions were able to access the CNS from extraneural entry sites. The initial prion replication site in the CNS can often be linked to the entry site by peripheral nerves, probably by retrograde axonal transport.⁵⁵ Experiments using hamsters demonstrated that

oral transmission of prion led to early prion deposition in enteric and autonomic ganglia as well as vagus and splanchnic nerves, and subsequently in the thoracic spinal cord and dorsal motor nucleus of the vagus in the brainstem, consistent with retrograde prion spread along autonomic peripheral nervous system (PNS) pathways into the CNS.⁵⁶ Similarly, prion inoculation into the mouse eye induces prion deposition along the optic nerve and tract, followed by the contralateral superior colliculus to which it projects.⁵⁷ Interestingly, prion conformation also plays a role in prion neuro invasion, as fibril-forming prions spread poorly to the brain compared to oligomeric or subfibrillar prions.^{58–60}

Recently, the discovery of prion in peripheral organs has opened the question about the spreading of PrP^{Sc} outside the CNS.⁶¹ The presence of prion was demonstrated by Western Blotting in many organs, including the spleen, and muscle,⁶² tonsil, and lymph node tissues.⁶³ Since then, the presence of peripheral PrP^{Sc} was detected only in cases of patients affected by vCJD. In recent studies, Western blotting analysis was used to detect PrP^{Sc} in the spleen of a sCJD patient, although the PrP^{Sc} levels were lower by a factor of approximately 10^{-4} than in brain tissue.⁶⁴ PrP^{Sc} was also detected, using in vitro amplification assays, in skin punches⁶⁵ and peripheral nerves⁶⁶ of patients affected by sCJD. These studies highlight the need to elucidate prion distribution in humans to reduce the risk of accidental prion infection. Moreover, they opened up the possibility of exploring these accessible tissues as novel biomatrices for the in vivo diagnosis of prion diseases.

Synucleinopathies

Synuclein protein family

In the second half of the '80s Maroteaux and colleagues first identified a neuron-specific protein of 143 amino acids (aa) in cholinergic vesicles and the nuclear envelope of the *Torpedo californica* and a highly homologous 140 amino acid protein in a rat brain. Because of the identification of the bulk of the protein in synaptic vesicles, they prompted the name *Synuclein*, whose localization was confirmed by other groups in subsequent years.^{67–70}

In 1993, Uéda and co-workers isolated a 35 amino acid peptide in the SDS-insoluble fraction of brain tissue from patients with Alzheimer's disease. They named this peptide the non-A β component of Alzheimer's disease amyloid (NAC). The precursor protein of this peptide, called NACP, the non- A β components precursor, was found to be homologous to rat α -synuclein.⁷¹

One year later, two proteins with a high homology level were purified from the human brain: a 140 aa that was found to be the human homologous of synuclein (=NACP), and the

phosphoneuroprotein14 (PNP-14), a 14 kDa phosphoneuroprotein found in bovine brain tissue identified by Nakajo et al.⁷² These human proteins were named α -synuclein and β -synuclein, respectively.⁷³

Later, a high level of a new member of the human synuclein gene family, γ -synuclein, was identified; it was principally expressed in the brain but also found to be overexpressed in ovarian cancer and carcinoma breast tissues.⁷⁴

α -synuclein

Of the three synuclein proteins, α -synuclein is probably the most studied, given its central role in the pathogenesis of a group of prevalent neurodegenerative diseases.⁷⁵ α -synuclein is a 140-amino acid protein encoded by the *SNCA* gene localized on the long arm of chromosome 4 (Chr 4q22.1).⁷⁶ The protein comprises an N-terminal region containing seven 11-residue repeats (1-95), including a highly conserved KTKEGV hexameric motif and the central amyloid-binding domain (NAC) and an acidic C-terminal region (residues 96-140) (Figure 5 A).^{77,78}

The amphipathic α -helical domains of 11-residue repeats are reminiscent of those included in apolipoproteins, which carry lipid molecules by reversibly binding to them.⁷³ Additionally, these repeat sequences also decrease the tendency of α -synuclein to form β -sheet structures, such as fibrils.⁷⁷⁻⁷⁹ The NAC region of α -synuclein (residues 61-95) is involved in forming fibrils due to its hydrophobic composition.⁷⁸ An acidic and glutamate-rich sequence characterizes the C-terminal domain (residues 96-140). It exhibits a random coiled-coil structure due to its hydrophobicity and negative charge, making this region involved in various interactions and modifications particularly relevant for physiological and pathological processes. The unstructured acidic and glutamate-rich C-terminal sequence of α -synuclein is subjected to multiple posttranslational modifications, including serine and tyrosine phosphorylation, ubiquitination, nitration, glycation, glycosylation, and C-terminal truncation. These modifications result in changes in protein charge and structure and alterations in binding affinities to other proteins and lipids. Although the phenomenon is still largely unexplored in the physiological context, it has become clear that such modifications may convert ordinary functions into pathological activities.^{79,80}

α -synuclein is a dynamic molecule whose secondary structure depends on its environment. In the soluble cytosolic state, it is intrinsically unstructured and behaves like a natively unfolded protein or, as it was recently shown in human erythrocytes, as a soluble, stable tetrameric form.^{81,82} In the membrane-bound state, α -synuclein can interact through the N-terminal lipid-binding domain with

lipid membranes such as vesicles, undergoing a major structural transition from random coil to the α -helical structure supporting the possible role of α -synuclein in lipid binding and transport. Additionally, it was shown that α -synuclein preferentially binds to vesicles of smaller diameter, hence the propensity to locate in synaptic vesicles in the brain.^{67,83–85} The various post-translation modifications, status, and localization of α -synuclein can explain the diverse cellular functions of this protein; it is involved in lipid transport, packing, and membrane biogenesis;^{86,87} it acts as a molecular chaperone;⁸⁸ it plays a role in vesicle trafficking,⁸⁹ and in synaptic plasticity.⁹⁰ Additionally, it was shown that α -synuclein could interact with several other proteins, although the physiological role of most of these interactions remains unclear.

α -synuclein is mainly concentrated in the presynaptic terminals in the peripheral and central nervous systems, in particular in the neocortex, hippocampus, striatum, thalamus, and cerebellum. This is in contrast to other proteins involved in neurodegeneration, which are mostly distributed throughout the neuron (e.g., cell body, dendrites, or axon).⁹¹ Additionally, α -synuclein localization is not limited to nervous tissues and CSF but can also be found in red blood cells, blood plasma, platelets, lymphocytes, blood vessels, testis, heart, lung, liver, kidney, and muscle.^{79,84}

Synucleinopathies and alpha-synuclein strains

Synucleinopathies are a group of disorders characterized by the accumulation of inclusions rich in the aggregated form of α -synuclein in neuronal and non-neuronal cells in the brain. The involvement of α -synuclein was demonstrated by Polymeropoulos and colleagues, who in 1997 first identified the A53T mutation in *SNCA*, the α -synuclein gene, in the Italian family, and three unrelated families of Greek origin with autosomal dominant inheritance for the PD phenotype.⁷⁵ In the same year, Spillantini et al. reported a strong immunoreactivity for α -synuclein in Lewy bodies (LBs) and Lewy neurites (LNs), abnormal neurites containing filaments, the hallmark of both PD and DLB pathology.⁹² LBs were first identified in dopaminergic neurons of substantia nigra by Fritz Jakob Heinrich Lewy as eosinophilic circular structures.⁹² Cytoplasmic inclusions containing α -synuclein are also the main histological hallmark of multiple system atrophy (MSA). However, they are typically localized in oligodendrocytes rather than neurons and, for this reason, are named glial cytoplasmic inclusions (GCIs) (Figure 5 B).

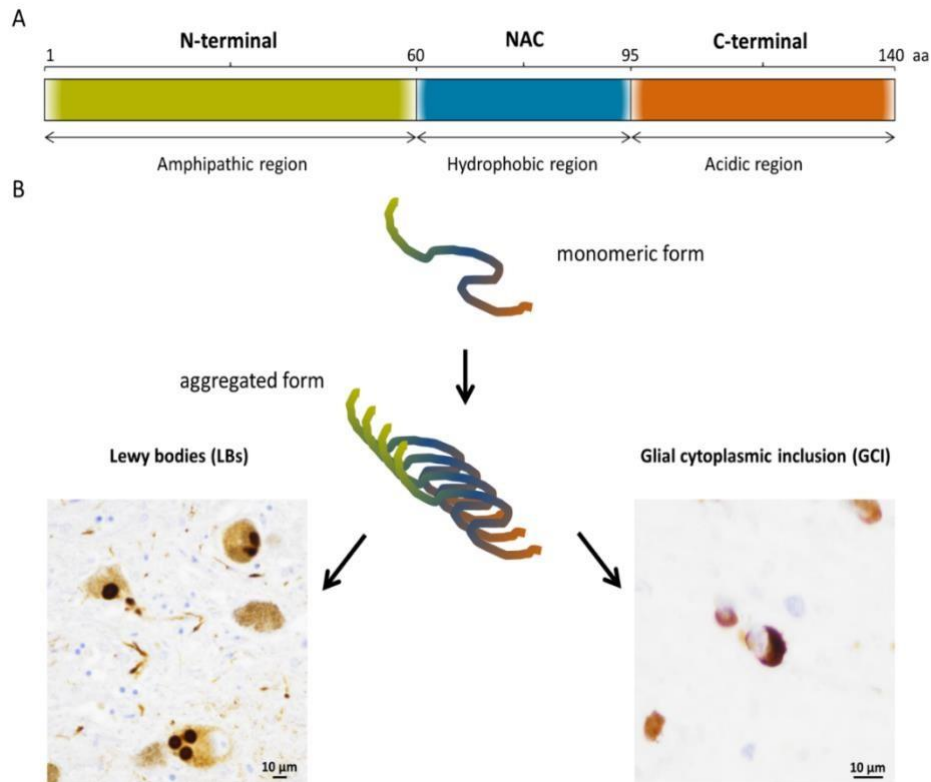


Figure 5. A) Primary structure of α -Syn protein characteristic domains: amphipathic, hydrophobic and acidic regions. B) Images of disease-specific lesions (LB and GCI) caused by pathological aggregation of α -Syn. Immunostaining was carried out with LB509 antibody (dilution 1:100, Thermo Fisher). Images were captured at 40X and 60X magnification.

While these pathologies share the proteinaceous origin and the symptoms may overlap, the pattern and severity of autonomic dysfunction with associated symptoms and clinical signs are different.⁹¹ This evidence led to the hypothesis of the existence, like in prion diseases, of α -synuclein strains.⁹³ Similar to PrP^{Sc}, it was suggested that recombinant α -synuclein monomers might also form synthetic α -synuclein aggregates with distinct conformations and biological activities.^{94–98} In physiological salt concentrations, α -synuclein monomers could generate aggregates with a cylindrical shape, named fibrils, and a flat structure, called ribbons. Subsequent studies demonstrated that these differences led to divergent biological activities, such as cytotoxicity and the ability to induce α -synuclein pathology in vivo.^{95,96} Prusiner and colleagues found that only pathological α -synuclein extracted from MSA patients, but not those of the other synucleinopathies, could propagate in α -Syn140*A53T–YFP mice.⁹⁹ Similarly, Yamasaki’s group demonstrated the presence of different inclusions in cells infected by PD and MSA α -synuclein aggregates.¹⁰⁰ These strain features were also confirmed by inoculation of preformed fibrils (PFF) or brain homogenates in animal models.^{98,99,101} In line with the above findings, Peng et al. reported a stronger seeding activity of MSA (GCI- α -Syn)

aggregates than PD (LB- α -Syn) ones, demonstrating the role of oligodendrocyte environment in the generation of GCl- α -Syn strain.¹⁰²

Recently, using fluorescent probes, NMR spectroscopy, electron paramagnetic resonance, and cryo-electron, differences in the conformational properties of PD and MSA α -synuclein extracts were confirmed.^{103,104}

Parkinson's disease

Parkinson's disease, first described by James Parkinson in 1817, represents the most prevalent synucleinopathy, affecting almost 200.000 people in Italy and a 14 per 10000 person-year incidence, which is strongly age-dependent.¹⁰⁵ The main PD symptoms are related to motor manifestations, including bradykinesia, rigidity, and rest tremor.¹⁰⁶ However, PD patients suffer several nonmotor symptoms such as cognitive decline, anxiety, depression, sleep disturbance, and dysautonomia. These symptoms may precede the onset of motor manifestation by as much as decades. Indeed, it is well documented that some clinical syndromes characterized by non-motor signs may represent the prodromal stage of PD or DLB. Specifically, the best known are pure autonomic failure (PAF), characterized by orthostatic hypotension and sphincteric disturbances, and idiopathic rapid eye movement (REM) sleep behavior disorder (RBD), showing abnormal movements in the absence of muscle hypotonia during REM sleep.^{107,108} The study of patients affected by these syndromes could help to identify patients with PD or DLB early.

Dementia also affects PD patients, with 50% and 83% of patients developing it 10 and 20 years after disease onset, respectively.^{109–111} The eponym PD Dementia (PDD) is assigned when dementia syndrome occurs more than one year after PD onset.¹¹²

Dementia with Lewy Body

Dementia with Lewy Body is the second most common synucleinopathy, with an incidence of 3.5 cases per 10000 person-year.^{113–115} DLB and PDD are two clinical syndromes that differ in the sequence of onset of dementia and parkinsonism, despite having a similar progression of the pathological changes. Consequently, these two syndromes can be viewed as a continuum rather than dichotomous entities. Specifically, patients that manifest dementia after one year from the onset of motor symptoms are classified as PDD, and subjects that develop dementia before or within one year from the diagnosis of PD are diagnosed as DLB.¹¹²

Disproportionate attentional and executive dysfunction with visual processing deficits, accompanied by progressive and severe cognitive decline, are required to diagnose DLB.¹¹⁶ Before the full development of DLB, the manifestation of one or more of the basic clinical features of the disease could occur usually accompanied by mild cognitive decline.¹¹⁷ Hence, the prodromal phases, referred to as pre-dementia stages with signs or symptoms predicting the future development of DLB, may consist of motor symptoms and signs, sleep disorders (i.e., RBD), autonomic dysfunction, and neuropsychiatric disturbances.¹¹⁸

REM sleep behavior disorder

RBD is a REM-phase associated parasomnia in which the normal muscle atonia of REM sleep is lost, and abnormal behaviours such as vocalisation and the realization of the dream occur. RBD can be classified as isolated (iRBD) or secondary (when a cause is identified). The latter is associated with a neurological disorder (e.g., neurodegenerative disorders, narcolepsy, or structural lesions in the brainstem), the introduction of certain drugs (e.g., antidepressant drugs or β blockers), and alcohol withdrawal.¹¹⁹ IRBD is usually diagnosed at 50–85 years of age with a male prevalence. The estimated duration of iRBD is about 1–10 years, but some patients report a history above 30 years.¹²⁰ The diagnostic criteria for RBD include a history of repeated episodes of sleep-related vocalisations, complex motor behaviours, or both, which often correlate with dream-enacting behaviours; behaviours that are documented to occur during REM sleep by polysomnography or presumed to occur in REM sleep by clinical history of dream enactment; and REM sleep without atonia as detected by polysomnography. iRBD represents the prodromal stage of the synucleinopathies since most IRBD patients are eventually diagnosed with PD, DLB, and occasionally with multiple system atrophy (MSA).^{121,122}

Alpha-synuclein cellular and tissue spread

As mentioned above, α -synuclein shares with PrP^{Sc} a similar aggregation mechanism placing synucleinopathies among the prion-like disorders. Additionally, it was demonstrated that the two proteins shared a common spreading mechanism. Early evidence supporting this theory came from the observation of α -synuclein aggregates in grafted fetal mesencephalic progenitor neurons several years after transplantation and implied host-to-graft Lewy pathology transmission.^{123,124} Since then, accumulating evidence has shown that α -synuclein seeds formed from recombinant proteins or lysates containing aggregates from diseased brains can propagate according to the

prion-like paradigm in neuronal cells, in organotypic slice cultures, and rodent models of PD.¹²⁵ Such evidence prompted further experimental studies to explore better how this spread can occur.^{126,127} Additionally, the prion-like spreading ability of the misfolded α -synuclein protein was reproduced with synthetic aggregates inoculated in animals or cellular models.^{128–131} Since the mechanism of α -synuclein diffusion from cell-to-cell is not entirely clear, several were hypothesized. It has been shown that small amounts of α -synuclein can be secreted through a vesicular mechanism and, in particular, through exosomes that are typically targeted for degradation into lysosomes.¹³² Jang et al. showed that vesicles not only preferentially secrete the misfolded α -synuclein but also increase the release process, suggesting a clearance mechanism of damaged proteins.¹³³ Once in the extracellular space, it was demonstrated that α -synuclein could be taken up by neighbouring cells in culture via several routes, including direct penetration of the plasma membrane, fluid-phase, or receptor-mediated endocytosis (e.g., via lymphocyte-activation gene in cultures of primary neurons) or fusion of plasma-exosomal membranes.^{134–138} The finding of a basal expression of α -synuclein and transfer of the protein from neuron-to-neuron or neuron-to-oligodendrocyte supported the hypothesis of oligodendrocytes involvement as a potential trigger of protein accumulation.^{126,139} Braak and colleagues demonstrated the involvement of dorsal motor and anterior olfactory nucleus in the early stage of PD, advancing the hypothesis that PD pathology might originate in the synapses of the peripheral nervous system (PNS), particularly from the enteric tract and subsequently spread in the CNS,¹⁴⁰ a piece of evidence supported by the finding of pathological α -synuclein aggregates in the PNS of PD patients up to 20 years before diagnosis.^{141–143} As is the case for PrP^{Sc}, it was shown that α -synuclein fibrils could also be transmitted by oral, intraperitoneal, intramuscular, and intravenous inoculation, leading to widespread α -synuclein pathology in the CNS of transgenic mice, enforcing the prion-like hypothesis.¹⁴⁴

Real-Time Quaking-Induced Conversion (RT-QuIC) assay

A brief history

In the attempt to better understand the mechanism of PrP conversion, in the mid '90s, Kocisko and colleagues successfully generated aggregated species of PrP in a cell-free assay. Based on the hypothesis of the ability of PrP^{Sc} to enroll and convert its physiological counterpart, an excess of PrP^{Sc} isolated from prion-infected hamsters was incubated with a 35S-labelled recombinant hamster PrP^C. The subsequent demonstration of proteinase K (PK)-resistant labeled PrP proved the de novo formation of misfolded species.¹⁴⁵ Then, following the fragmentation-nucleation hypothesis as the

mechanism of PrP^c conversion and aggregates formation, cyclic sonication and incubation steps were added to the reaction to increase its efficacy; this assay was named Protein Misfolding Cyclic Amplification (PMCA).¹⁴⁶ Although the assay was able to detect the presence of small amounts of PrP^{Sc} in the brain even in the pre-symptomatic phase,¹⁴⁷ rendering this method essential for both research and diagnostic application, it had some limitations. The preservation of infectiveness of end-products and sensitivity to contaminants posed the question of the application in routine clinical practice and the research of new technical improvements to find a more reproducible and less time-consuming protocol (i.e. the assay required many sonication cycles and the presence of PK resistant PrP^{Sc} was assessed by Western Blot analysis).^{146,148} Later, Atarashi and co-workers improved the reproducibility compared to PMCA. They reduced the time required for additional aggregate formation by using bacterially expressed recombinant PrP as the reaction substrate (instead of brain homogenate) and an automated shaking, developing the first QuIC assay.¹⁴⁹ In 2010, combining the QuIC cyclic amplification with the real-time detection of the products by thioflavin T (ThT), introduced by Colby et colleagues,¹⁵⁰ Wilham developed the currently used Real-Time Quaking-Induced Conversion, RT-QuIC, set-up¹⁵¹ (Figure 6).

The ability to detect minute amounts of PrP^{Sc} was successively confirmed in the application of the assay to cerebrospinal fluid (CSF) and other non-nervous tissues of animals and humans affected by prion diseases.^{152–158}

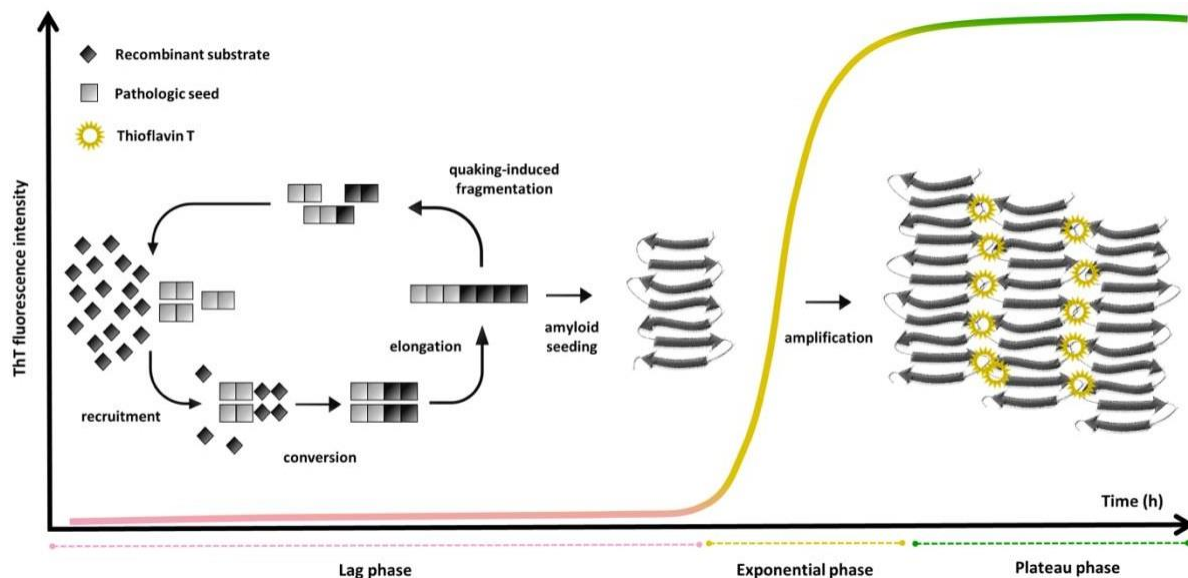


Figure 6. Schematic illustration of the RT-QuIC assay. The RT-QuIC reaction phases may be summarized in lag phase, exponential phase and plateau phase. During the former step, seeds structurally convert the protein recombinant substrate triggering a protein aggregation. With the formation of the first fibrils the system detects the fluorescent signal of ThT, a dye with a strong affinity with the fibrillar protein state (exponential phase). Eventually, when all the substrate is incorporated into fibrils, a plateau phase is observed. The figure was adapted from Candelise et al., *Acta Neuropath Commun* 2020.¹⁵⁴

The need for new early biomarkers for neurodegenerative diseases

Since the development of prion RT-QuIC, based on the shared aggregation mechanism among the best-known proteins associated with neurodegeneration, including β -amyloid, tau, α -synuclein, and TDP-43, researchers attempted to expand the application of the assay to the early diagnosis of prion-like neurodegenerative disorders.¹⁵⁹

In neurodegenerative diseases, where post-mortem neuropathologic examination remains the gold standard for a definite diagnosis, the success of prion RT-QuIC has strongly suggested further developments of the assay and application to the full spectrum of neurodegenerative disorders. The potential diagnostic value of RT-QuIC is strengthened by the fact that current diagnostic criteria usually require the combination of multiple diagnostic investigations, clinical findings, and an adequate follow-up of several years to identify the disorder accurately.¹⁶⁰ Additionally, imaging, neuropsychological and neurophysiological examinations are often only supportive of the clinical findings, and currently used CSF biomarkers like total tau, 14-3-3, and neurofilament proteins, only reflect neuronal damage and, for this reason, do not describe a specific pathology but support the clinical picture.^{155,161}

RT-QuIC assay across prion diseases

Early diagnosis of CJD is challenging due to the wide clinical heterogeneity at disease onset, with large overlaps with that of other rapidly progressive dementias (RPDs), and the variable disease progression affecting survival times.¹⁶² Over the past 15-20 years, brain-derived CSF protein assays that serve as surrogate markers for neuronal damage and diffusion-weighted magnetic resonance imaging (DW-MRI) have provided the main support for clinical diagnosis, demonstrating, however, incomplete diagnostic accuracy with significant variability across disease subtypes.¹⁵⁷ Additionally, in the absence of a post-mortem neuropathological examination, an unknown number of atypical prion cases skip recognition. The introduction of the RT-QuIC assay provided a reliable and robust tool to improve the early diagnosis of human prion diseases.^{11/02/2023 17:02:00} The so-called first-generation RT-QuIC (also termed PQ-CSF), which uses a recombinant full-length hamster prion protein (Ha23–231) as substrate, demonstrated a 73–100% sensitivity and, most significantly, a 98–100% specificity in CJD, a result validated by several laboratories.^{153–155,163–165} The assay showed good reproducibility in the interlaboratory setting and under various CSF storage conditions.^{166,167} Using a chimeric version of PrP or the *Bank vole* prion protein (BV23-230) rather than wild-type hamster PrP as substrate yielded similar diagnostic accuracy in both genetic and sporadic CJD.^{168–170} Protocol modifications, particularly the use of the truncated form of hamster PrP (Ha90-231) as substrate, which resulted in second-generation RT-QuIC (also termed improved QuIC CSF, or IQ-CSF), allowed the experimental run time to be reduced to 1–2 days and lead to a further overall increase in the sensitivity at 92-100% without affecting specificity.¹⁷¹ Two independent studies specifically compared the first and second-generation RT-QuIC in the same patient population, and both confirmed the higher sensitivity of the IQ-CSF compared to the first-generation assay.^{156,172} In summary, regardless of the type of protocol (Table 2), all studies conducted to date have demonstrated the remarkable added diagnostic value of prion RT-QuIC compared to surrogate biomarkers.¹⁵⁷

RT-QuIC assay across synucleinopathies

Like prion diseases, synucleinopathies are also widely heterogeneous in clinical manifestation, response to therapy, and rate of progression, making early diagnosis difficult, which is further complicated by overlapping symptoms with atypical parkinsonisms such as progressive supranuclear palsy (PSP) and corticobasal degeneration (CBD), two primary tauopathies, and other neurodegenerative dementias such as AD or frontotemporal dementia (FTD). Additionally, the recognition that two rare syndromes, pure autonomic failure (PAF) and isolated rapid eye movement (REM) sleep behavior disorder (iRBD), characterized by the early α -synuclein accumulation in the peripheral autonomic system and lower brainstem, represent prodromal syndromes of both MSA and LB-related disorders (LBD), has broadened the clinical spectrum of

synucleinopathies.^{173,174} Because of this heterogeneity, the clinicopathological rate of accordance in autopsy-verified cohorts remains partially inaccurate (i.e., 92.6% for PD, 81.6% for DLB, 62–78.8% for MSA).^{175–177}

Fairfoul and colleagues were the first to apply the RT-QuIC to the CSF of 20 clinically diagnosed PD and 12 neuropathologically confirmed DLB cases. This α -syn RT-QuIC showed a 100% specificity and 92–95% sensitivity. Interestingly, three samples derived from patients affected by iRBD also gave a positive result, providing preliminary evidence that RT-QuIC may predict the future onset of synucleinopathy in patients affected by prodromal syndromes.¹⁷⁸ Later, Soto's group obtained similar results using an adopted version of the previously reported prion PMCA assay, obtaining a sensitivity of 88% and a specificity of 97%.¹⁷⁹

In recent years, many groups validated the application of α -Syn RT-QuIC for the diagnosis and discrimination of synucleinopathies. In particular, Rossi and colleagues applied the standard protocol developed by Caughey's lab but using a wild-type recombinant α -synuclein substrate instead of the mutant form used by Groveman et al.¹⁸⁰ to the largest cohort of CSF samples examined to date. They included 439 clinically well-characterized, or post-mortem verified patients with parkinsonism or dementia and, for the first time, a significant number of patients with iRBD and PAF. The RT-QuIC assay detected α -synuclein seeding activity across the entire spectrum of LBD investigated with an overall sensitivity of 95.3% and a 98% specificity.¹⁸¹ Despite the enormous success, the α -Syn RT-QuIC protocols still differ among the laboratories, with several assay variables remaining to explore.

RT-QuIC biomatrices across prion diseases and synucleinopathies

Currently, CSF is the matrix of choice for the prion and α -syn RT-QuIC. This is due to the high performance of the CSF assay, its accessibility as a fluid proximal to the brain, where protein aggregates predominantly accumulate, and the systematic collection of this biofluid in patients with RPDs for diagnostic purposes.

However, despite the highly dominant tropism for the CNS, it is well-established that both PrP^{Sc} and α -synuclein aggregates can also accumulate in extra-neural tissues. Regarding prion diseases, the relatively low amount of PrP^{Sc} deposition in peripheral tissues requires the use of ultrasensitive techniques, like enhanced chemiluminescence,^{182–186} tissue precipitation with sodium phosphotungstic acid,^{183,187} or other concentration/purification protocols.^{182,185,186} Using these strategies, several groups detected PrP^{Sc} in the olfactory and retinal epithelium, cranial and

peripheral nerves, muscles, skin, and spleen of sCJD patients. The introduction of RT-QuIC opened the way for the application of the test to accessible peripheral tissues collected *in vitam*. In this perspective, different studies demonstrated the presence of PrP^{Sc} aggregates in several peripheral tissue homogenates like olfactory mucosa (OM),^{154,163,188} and skin punch biopsy.¹⁸⁵

Orrù et al. demonstrated positive RT-QuIC results on multiple eye components taken post-mortem, including the retina, optic nerve, extraocular muscle, choroid, lens, vitreous, and sclera of 11 sCJD patients.¹⁸⁹ In addition to cranial nerves, prion seeding activity was demonstrated in peripheral nerves (sural, sciatic, femoral, and common peroneal) collected post-mortem from one gCJD-V210I and 11 sCJD individuals.¹⁸⁶ Moreover, observation of prion seeding activity in the skin of scrapie-infected hamsters and transgenic mice before the appearance of clear clinical signs of infection suggests that skin punch biopsies could be relevant for preclinical diagnosis of human prion disease, particularly in subjects at genetic risk for the disease.¹⁹⁰

Following the successful application of PrP RT-QuIC on peripheral tissues, several groups used RT-QuIC to detect misfolded forms of α -synuclein in olfactory mucosa,^{191–193} skin,^{194,195} saliva,¹⁹⁶ and gastrointestinal tract (GI).¹⁹⁷

However, in contrast to the high accuracy in prion disease, α -syn RT-QuIC using OM showed a suboptimal performance (65.5%-84% sensitivity and 84.4-85,7% specificity).^{191,198} Other biological samples, including post-mortem skin punches, were also examined with α -syn RT-QuIC. These studies have shown promising results for the use of skin punches as a relatively non-invasive biomarker for the detection of synucleinopathies.^{194,195} The application of RT-QuIC on easily obtainable biofluid and tissue specimens will be an important step in the development of robust diagnostic biomarker assays for various neurodegenerative disorders to further study disease progression, co-pathologies and potential treatments.

Ph.D. RESEARCH PROJECT

The laboratory of Neuropathology at ISNB (Bologna, Italy) is currently a worldwide leader in the application of prion and α -syn RT-QuIC. The purpose of this project was to compare the diagnostic performance of skin and CSF RT-QuIC to use skin biopsies as a less invasive and more reliable alternative biomatrix for both prion and α -syn RT-QuIC. The results were published in two recent publications that showed the higher sensitivity and specificity of skin RT-QuIC:

- Mammana, Angela, et al. "Detection of prions in skin punch biopsies of Creutzfeldt-Jakob disease patients." *Annals of clinical and translational neurology* vol. 7,4 (2020): 559-564. doi:10.1002/acn3.51000.¹⁹⁹
- Mammana, Angela, et al. "RT-QuIC Detection of Pathological α -Synuclein in Skin Punches of Patients with Lewy Body Disease." *Movement disorders: official journal of the Movement Disorder Society* vol. 36,9 (2021): 2173-2177. doi:10.1002/mds.28651.²⁰⁰

Another publication, "*Misfolded α -synuclein assessment in skin and CSF by RT-QuIC in isolated REM sleep behavior disorder*" in collaboration with Dr. Alex Iranzo from the Neurology Service, Multidisciplinary Sleep Unit, Hospital Clinic de Barcelona, IDIBAPS, CIBERNED, Barcelona, Spain, in which skin RT-QuIC was used to assess the presence of α -synuclein aggregates in skin biopsies in patients affected by iRBD, is under submission.

MATERIALS AND METHODS

Mammana, Angela et al. “Detection of prions in skin punch biopsies of Creutzfeldt-Jakob disease patients.”

CJD patients and controls

Seventy-one punch biopsies from patients referred to the Laboratory of Neuropathology, Institute of Neurological Sciences of Bologna (ISNB), were analysed. The cohort included a series of 57 patients with post-mortem neuropathological assessment (i.e., “neuropathological” [NP] cases) referred to our lab because of the clinical suspicions of CJD. Specifically, it includes 35 patients with definite CJD and 22 non-CJD patients with neurological disorders of different etiology. An additional cohort of 5 patients underwent *in vitam* skin biopsy, including 3 patients with clinical suspicions of sCJD (probable sCJD), 2 with a definite sCJD diagnosis and a control group of 15 patients who were investigated for small-fiber neuropathy (diabetic neuropathy [n = 3], idiopathic small fiber neuropathy [n = 4], pure autonomic failure [n = 1], Parkinson’s disease [n = 2], Alzheimer’s disease [n = 2], and Dementia with Lewy bodies [n = 3]). Forty-one patients from both cohorts underwent a diagnostic Lumbar puncture (LP) *in vitam* and had CSF available for the RT-QuIC, in addition to skin samples. They included 26 patients with a definite diagnosis of sCJD (23) or gCJD (3), 3 with a clinical diagnosis of CJD, 11 non-CJD, and 1 clinical control. Prion disease (n = 35) was diagnosed according to the current European criteria for CJD (<https://www.cjd.ed.ac.uk>). Molecular analysis of *PRNP*, PrP^{Sc} typing, subtype classification, and results of the diagnostic investigation are described in Table 2.

Table 2. Demographic features and results of diagnostic investigations in the tested patient cohort

Final diagnosis	n	Mean, SD		CSF		Brain MRI	EEG
		Age at onset, y	Disease duration, mo	14-3-3 protein ^a positive /tested (%)	t-tau ^b >1250 pg/ml positive/tested (%)	Positive ^c / tested (%)	PSWCs/ tested (%)
Definite sCJD	29	70.8±10.8	8.2±9.3	19/23 (82.6)	23/24 (95.8)	20/25 (80.0)	18/26 (69.2)
MM1	21	70.7±11.4	6.2±9.2	14/17 (82.4)	18/18 (100)	13/18 (72.2)	16/19 (84.2)
VV2	3	70.0±14.5	8.9±4.8	1/1 (100)	1/1 (100)	3/3 (100)	1/3 (33.3)
MV2K	2	72.5±7.8	10.3±7.3	2/2 (100)	2/2 (100)	2/2 (100)	0/2 (0.0)
MM2C	3	70.7±8.1	20.5±8.9	2/3 (66.7)	2/3 (66.7)	2/2 (100)	1/2 (50.0)
Probable sCJD	3	64.0±3.6	7.8±6.0	2/3 (66.7)	1/1 (100)	3/3 (100)	0/1 (0.0)
MM	1	60.0	NA ^d	1/1 (100)	1/1 (100)	1/1 (100)	0/1 (0.0)
MV	1	65.0	12.0	0/1 (0.0)	1/1 (100)	1/1 (100)	0/1 (0.0)
VV	1	67.0	3.5	1/1 (100)	1/1 (100)	1/1 (100)	0/1 (0.0)
Genetic CJD	3	70.0±8.9	5.7±6.9	3/3 (100)	3/3 (100)	2/2 (100)	1/3 (33.3)
E200K-129M	2	65.0±2.8	8.1±7.9	2/2 (100)	2/2 (100)	2/2 (100)	1/2 (50.0)
V210I-129M	1	80.0	1.1	1/1 (100)	1/1 (100)	Na	0/1 (0.0)
Non-CJD	37	67.8±10.9	25.2±49.7^e	7/12 (58.3)	5/14 (35.7)	5/21 (23.8)	0/18 (0.0)

^aEvaluated semi-quantitatively by Western blotting as described.¹⁵⁵ ^bMeasured quantitatively by ELISA as described.¹⁵⁵ ^cAccording to the current European diagnostic criteria for CJD diagnosis.¹⁵⁵ ^dThe patient is still alive. ^eCalculated in the patient group referred for suspected CJD.

List of abbreviations: CSF, cerebrospinal fluid; MRI, magnetic resonance imaging; EEG, electroencephalography; PSWCs, periodic sharp-waves complexes; sCJD, sporadic Creutzfeldt-Jakob disease; FFI, fatal familial insomnia; Na, not available.

Neuropathological examination

Neuropathological examination was performed using standardized procedures according to the autopsy protocol of the Laboratory of Neuropathology at ISNB.¹⁵⁵ Briefly, the brain was sagittally divided into the two hemispheres: the right half was sectioned coronally and then immediately frozen at – 80 °C in sealed plastic bags, while the left hemisphere was fixed in 10% buffered formalin and then serially sectioned in 1 cm slices, and regionally sampled in tissue blocks according to standardized procedures.²⁰¹ Seven µm thick sections from each block were stained with hematoxylin-eosin for screening. Moreover, immunohistochemistry with antibodies specific for PrP

(3F4, dilution 1:400, Signet Labs), α -synuclein (LB509, dilution 1:100, Thermo Fisher Scientific, and KM51, dilution 1:500, Novocastra), hyperphosphorylated tau (AT8, dilution 1:100, Innogenetics), and A β (4G8, dilution 1:5000, Signet Labs) was performed to all cases using different brain regions, mainly following established consensus criteria.^{202–204} An experienced neuropathologist (Prof. Piero Parchi) formulated the final diagnosis, assigned the Braak stage of LB-related pathology,²⁰⁴ and classified each case according to the level of AD neuropathologic change (ABC score).^{162,203,205}

CSF collection and analyses

CSF samples were obtained by LP at the L3/L4 or L4/L5 level following a standard procedure. Specimens were centrifuged in case of blood contamination, divided into aliquots, and stored in screw cap polypropylene microtubes at $-80\text{ }^{\circ}\text{C}$, until analysis.

Levels of t-tau, p-tau, A β 42, and A β 40 in CSF were measured by automated chemiluminescent enzyme immunoassay (CLEIA) on the Lumipulse G600 platform (Fujirebio, Gent, Belgium). Analysis of 14-3-3 protein was performed by Western Blot, as previously described.¹⁵⁵ Brain diffusion weighted-MRI (DW-MRI) findings were considered positive when showing (either in DW or FLAIR sequences) a hyperintensity in the striatum or at least two cortical regions.²⁰⁶

Skin biopsy procedure and sample preparation

Skin tissues were collected in the cervical C7 paravertebral area (proximal site) and/or in the lateral surface of the thigh (~ 20 cm above the patella) (distal site).²⁰⁷ *Ex vivo* samples were collected at autopsy before opening the skull to avoid cross-contamination with brain tissue. In living patients, 3-mm punch biopsies were taken after cleansing the skin with povidone and applying topical anaesthesia under lidocaine (20 mg/mL) and epinephrine (0.0125 mg/mL) using a sterile technique according to the European Federation of Neurological Societies and Peripheral Nerve Society guidelines.²⁰⁸ Skin samples consisted of 3-mm wide and 5-mm deep cylinders, which included the epidermis and dermis. No suture was required, and lesions were allowed to heal by granulation and re-epithelialization.

Skin punches collected post-mortem and in living patients were frozen immediately at $-80\text{ }^{\circ}\text{C}$ after collection.

Following thawing, samples were washed three times in PBS 1X to remove any impurities and contaminants such as traces of blood. Then, they were homogenized at 1% (w/v) with gentle-MACS Octo Dissociator (Miltenyi BioTec) in cold QuIC buffer containing 150 mmol/L NaCl, 4 mmol/L EDTA, 1x PBS, and Complete Protease Inhibitor Mixture. The brain of a sCJDV2 and an AD subject, used

as additional positive and negative controls, were homogenized at 10% by adding 1% Triton X-100 at QuIC buffer. Skin homogenates were then centrifuged at 1000xg for 10 min at 4°C, and supernatants were stored at -80°C until use.

Prion RT-QuIC

Skin samples were analysed with RT-QuIC using two different substrates, namely full-length rec-PrP *Syrian hamster* (Ha23-231) and *Bank vole* (Bv23-230). The latter was produced in-house, while Ha23-231 was obtained by Dr. A. Green, University of Edinburgh. Both substrates were purified according to a previously published protocol.^{164,209} After thawing, supernatants were serially diluted in 1X PBS with 0.1% or 0.05% Sodium dodecyl sulfate (SDS) for Ha23-231 and Bv23-230, respectively, supplemented with N2 media [Gibco]. Two μL of 10^{-3} diluted samples were added to 98 μL of the reaction mix containing 10 mM phosphate buffer (pH 7.4), 130 mM NaCl, 0.1 mg/ml recombinant Ha23-231 or Bv23-230 prion protein, filtered with a 100-kDa MWCO filter (Amicon Centrifugal Filters, Merck Millipore, Burlington, Massachusetts, USA), 10 μM Thioflavin T (ThT), 1 mM ethylenediaminetetraacetic acid tetrasodium salt hydrate (EDTA) at pH 8.0 and loaded in quadruplicate in a black 96-well plate with a clear bottom (Nunc). All the reaction solutions were freshly prepared and filtered before use with 0.22 μm sterile filters. After sealing with a plate sealer film (Nalgene Nunc International), the plate was incubated at 42 °C in a FLUOstar OMEGA reader (BMG, Germany) over a period of 60 h with intermittent cycles of shaking (60 s, 700 rpm, double-orbital) and rest 60 s, as previously described.^{169,185} The fluorescence intensity of ThT-PrP^{Sc} aggregates, expressed as relative fluorescence units (RFU), was detected every 45 min with a gain of 2000 for Ha23-231, and of 1600 for Bv23-230. Sample was considered prion-positive if at least two out of four sample replicates gave a fluorescence signal higher than the threshold cut-off value. This threshold indicated the mean of RFU values of all negative samples at 60 h plus 5 or 20 standard deviations for Ha23-231 and Bv23-230, respectively. For the CSF RT-QuIC, 15 μL of each CSF sample was added to 85 μL of reaction mix in the 96-well microplates as described in Franceschini et al.¹⁵⁶ Briefly, samples were tested in quadruplicate together with positive (definite CJD) and negative (non-CJD) controls. The RT-QuIC reaction mix consisted of 10 mM phosphate buffer at pH 7.4, 300 mM NaCl, 1 mM EDTA at pH 8.0, 10 μM ThT, 0.002% of SDS, and 0.1 mg/ml of *Syrian hamster* truncated form of prion protein (Ha90–231). After sealing, the plate was incubated in a FLUOstar OMEGA read at 55 °C and the fluorescence intensity of ThT-PrP^{Sc} aggregates was taken with a bottom read and a gain of 1000. A CSF sample was considered prion positive if at least two out of

four sample replicates gave a fluorescence signal higher than the threshold cut-off value. This threshold represents the mean RFU values of negative samples plus at least 10 standard deviations. For both biomatrices, samples were considered negative if none of the replicates surpassed the chosen cut-off. If only one of four replicates crossed the threshold, the test was considered ambiguous/unclear and repeated. The following parameters were used to quantitate the RT-QuIC output: the time taken to reach the threshold (lag phase) and the maximum fluorescence read (ThT max).

Statistical analysis

RT-QuIC relative fluorescence responses were analysed and plotted using Sigma Plot software (Systat Software Inc., Chigago, IL). The Mann–Whitney test was used to reveal differences between two groups; a P value <0.05 was considered statistically significant. Unless stated otherwise, data are expressed as mean ± standard error of the mean (SEM)

Mammana, Angela, et al. “RT-QuIC Detection of Pathological α -Synuclein in Skin Punches of Patients with Lewy Body Disease.”

LBD patients and controls

A consecutive series of 49 neuropathologically verified cases submitted to the Neuropathology laboratory at ISNB between 2018 and 2020, was analysed; this included 47 patients with rapidly progressive neurological syndromes of different etiology, of which 7 had incidental LB pathology (Table 4), 1 patient with dementia with Lewy bodies (DLB) and 1 with Parkinson’s disease (PD). In addition to the above NP cohort, skin punch biopsies from 28 patients fulfilling the clinical diagnosis of probable or clinically established PD or probable DLB and an additional control group of 41 patients affected by various neurological disorders, were analysed with α -Syn RT-QuIC assay. All patients with LBD were diagnosed according to Movement Disorder Society Clinical Diagnostic Criteria for PD and DLB Consortium Criteria. Seventy-nine patients belonging to both cohorts underwent a diagnostic LP *in vitam*; they included 18 patients with a clinical diagnosis of PD (7) or DLB (11), 1 with a post-mortem diagnosis of DLB, and 60 patients with various neurological disorders.

Table 3. Demographic features of the LBD studied cohort

Variable	In <i>vitam</i>			Post-mortem		
	DLB	PD	Controls	DLB, PD	Incidental LBD	Non-LBD
N	15	13	41	2	7	40
Age at biopsy or death (years)	75.0±7.9	68.2±6.7	66.8±11.4	79, 67	74.6±8.3	71.0±8.7
Time from onset to biopsy (years)	3.9±2.8	3.3±2.2	-	17.8, 17.0	-	-

Years are expressed as mean ± standard deviation. List of abbreviations: DLB, dementia with Lewy bodies; iLBD, incidental Lewy body disease; PD, Parkinson's disease

Skin biopsy procedure and sample preparation

The sampling protocol differed between the two cohorts. In the NP group, 3-mm punches were available for both cervical and thigh sites, except for 2 patients in whom only the cervical sample was collected. Samples collected in *vitam* were taken, with the same procedure used for the CJD patients, from a single site: the cervical region in 23 patients, the leg in 24, and the thigh in 22.

In both groups, samples, after being washed three times in 1X PBS, were homogenized at 1% (w/v) in cold 1x PBS supplemented with Complete Protease Inhibitor Mixture (Roche, Basel, Switzerland), centrifuged at 1000 xg for 10 min at 4°C and supernatants were stored at -80°C until use. A second 3-mm punch, taken at the same time and from the same site as the first one, was available in 17 (cervical), 21 (leg), and 18 (thigh) patients, respectively.

Neuropathological studies and CSF collection were performed as described above.

α -Syn RT-QuIC

Black 96-well plates with a clear bottom (Nalgene Nunc International) were pre-loaded with six 0.8 mm silica beads (OPS Diagnostics) per well.

After thawing, 2 μ l of homogenate skin samples at a final dilution of 10⁻² (w/v) were added to a 98 μ l of reaction mix containing 40 mM PB, pH 8.0, 170 mM NaCl, 10 μ M ThT, and 0.1 mg/ml of K23Q recombinant α -syn, produced in house, as described by Rossi et al, filtered using a 100 kDa MWCO filter (Amicon centrifugal filters, Merck Millipore).

CSF samples were thawed and vortexed 10 s before use. Fifteen μ L of CSF were added to 85 μ L of the reaction mix containing 40 mM PB, pH 8.0, 170 mM NaCl, 10 μ M ThT, 0.0015% SDS, and 0.1 mg/ml of wild-type recombinant α -synuclein filtered using a 100 kDa MWCO filter (Amicon centrifugal filters, Merck Millipore).

For both skin and CSF RT-QuIC, the plate was sealed and incubated into Fluostar Omega (BMG Labtech) plate reader at 42 °C with intermittent double orbital shaking at 400 rpm for one minute, followed by 1-min rest. ThT fluorescence measurements were taken every 45 min. To overcome possible batch-to-batch variations of α -synuclein activity and intrinsic plate-to-plate experimental variability, relative fluorescent units for every time point were normalized for the maximum intensity reached by the positive control and expressed in percentage.

Samples were run in quadruplicates and deemed positive when at least 2 out of 4 replicates reached the threshold. The threshold set at 15% indicates the lowest value that ensures clear discrimination between positive and negative replicates. The value corresponds to the mean of the signal of negative controls plus approximately 10 SD. The threshold is calculated separately for each 96-well plate to also limit the possible inter-experimental variability related to the use of different plate readers.²¹⁰ As positive controls, we used a skin sample from the patient with a definite post-mortem diagnosis of DLB included in the study, and a pool of CSF samples from a previous study, showing a complete 4/4 positive response. Samples giving a positive signal in a single replicate were classified as “unclear,” repeated up to three times, and finally considered negative unless giving a definite positive response.

Statistical analysis

RT-QuIC relative fluorescence responses were analysed and plotted using GraphPad Prism 8.4.0 for Windows. The Mann-Whitney test was used to reveal differences between two groups; the Fisher’s exact test was used to compare the proportion of 4/4 positive replicates between skin and CSF RT-QuIC outcomes; the unpaired Student T test was used to compare RT-QuIC quantitative values between two groups; p value <0.05 was considered statistically significant. Unless stated otherwise, data are expressed as mean with standard error of the mean (SEM).

Alex Iranzo, Angela Mammana, et al. “Misfolded α -synuclein assessment in skin and CSF by RT-QuIC in isolated REM sleep behaviour disorder”

iRBD patients and controls

Participants were recruited at the Hospital Clinic de Barcelona (HCB), Spain, where they underwent skin punch biopsy and lumbar puncture procedures the same morning. The study was prospectively performed between May 2021 and June 2022. During this period, all consecutive individuals with

polysomnographically confirmed iRBD who attended their scheduled visits at the sleep center of the HCB were invited to participate (n=134). Patients were asked to undergo extensive clinical assessment, neurological examination, and a series of tests and ancillary tools. Diagnosis of iRBD required chronic history of dream-enacting behaviors, video-polysomnographic confirmation of iRBD showing excessive electromyographic activity during REM sleep associated with abnormal behaviors, and absence of Parkinsonism, dementia, and coexistent neurodegenerative diseases. Of the 134 eligible iRBD patients, 91 agreed (Table 5) to participate, 33 declined, and 10 were excluded because of receiving anticoagulant therapy. A control group (n= 41) of healthy subjects plus individuals attending our sleep center who had sleep disorders not associated with the development of neurodegenerative disease (e.g., obstructive sleep apnea, insomnia), underwent simultaneous biopsy of the skin and LP the same day. In all controls, iRBD was excluded by clinical history and video-polysomnography showing REM sleep with muscle atonia. At the time of skin biopsy and lumbar puncture, controls had neither motor nor cognitive complaints, and their neurological examination was unremarkable. Exclusion criteria for all participants were disorders affecting the skin, coagulation abnormalities, use of anticoagulants, chemotherapy treatment, and allergy to lidocaine. For three patients (3.3%) and one control (2.4%), only skin biopsy was available because patients refused to undergo lumbar puncture.

Table 4. iRBD demographic founding

	iRBD (n=91)
Age at IRBD diagnosis (y)	66.1 ± 7.8
Age at lumbar puncture (y)	69.6 ± 8.4
Interval between IRBD diagnosis and lumbar puncture (y)	3.5 ± 3.8
Mean prodromal Parkinson disease probability at the time of lumbar puncture (%)	79.5 ± 31.9
Prodromal Parkinson disease probability ≥80% at the time of lumbar puncture, n (%)	66 (72.5)
Abnormal DAT-SPECT, n (%)	52 (57.1)
MDS-UPDRS-III score, n	1.9 ± 2.5
UPSIT-40 score, n	20.2 ± 7.1
UPSIT-40 score <18, n (%)	39 (44.3)
Depression, n (%)	34 (37.4)
Constipation, n (%)	50 (55.6)
Mild cognitive impairment, n (%)	12 (13.2)

Data are presented as number, percentage, mean and standard deviation.

List of abbreviations: IRBD= isolated rapid eye movement sleep behaviour disorder; DAT-SPECT= dopamine transporter imaging single photon emission computed tomography; MDS-UPDRS III= motor part of the Movement Disorders Society Unified Parkinson Disease Rating Scale; UPSIT= Spanish version of the 40 item University of Pennsylvania Smell Identification Test.

Skin biopsy procedure and sample preparation

Skin samples were collected, as previously described, from each side, right and left; specifically, four samples were collected from the posterior cervical paravertebral area (C7 and C8) and one from each leg. The C7 and C8 spinous processes were localized by manual palpation, and punches were performed on the left and right sides, 2.5-5 cm separated from the midline at each cervical level. The right and left leg biopsies were obtained 10 cm above the external malleolus. Each skin sample was placed in a different 1.5 mL tube and immediately frozen on dry ice. After 30 min of skin sample collection, the skin samples were stored at -80°C until they were shipped on dry ice to the ISNB. Once at ISNB, skin samples were washed three times in cold 1X PBS and homogenized at 1% (w/v)

with a gentleMACS Octo Dissociator (Miltenyi BioTec, Bergisch Gladbach, Germany) in cold 1X PBS supplemented with Complete Protease Inhibitor Mixture (Roche, Basel, Switzerland). Skin homogenates were then centrifuged at 1000xg for 10 min at 4°C, and supernatants were stored at -80°C until use.

α -Syn RT-QuIC

Both skin and CSF RT-QuIC were performed as the LBD cohort, as previously reported. Briefly, black 96-well were pre-loaded with six 0.8 mm silica beads (OPS Diagnostics) per well.

After thawing, 2 μ l of homogenate skin samples at a final dilution of 10^{-2} (w/v) were added to a 98 μ l of reaction mix containing 40 mM PB, pH 8.0, 170 mM NaCl, 10 μ M ThT, and 0.1 mg/ml of wild-type recombinant α -synuclein, produced in house, as described by Rossi et al, filtered using a 100 kDa MWCO filter (Amicon centrifugal filters, Merck Millipore).

CSF samples were thawed and vortexed 10 s before use. Fifteen μ L of CSF were added to 85 μ L of the reaction mix containing 40 mM PB, pH 8.0, 170 mM NaCl, 10 μ M ThT, 0.0015% SDS, and 0.1 mg/ml of recombinant α -synuclein filtered using a 100 kDa MWCO filter (Amicon centrifugal filters, Merck Millipore,).

For both skin and CSF RT-QuIC, the plate was sealed and incubated into Fluostar Omega (BMG Labtech) plate reader at 42 °C with intermittent double orbital shaking at 400 rpm for one minute, followed by 1-min rest. ThT fluorescence measurements were taken every 45 min. To overcome possible batch-to-batch variations of α -synuclein activity and intrinsic plate-to-plate experimental variability, relative fluorescent units for every time point were normalized for the maximum intensity reached by the positive control and expressed in percentage.

To overcome the intrinsic plate-to-plate variability and batch-to-batch variations, we normalized the relative fluorescent units for every time point for the maximum fluorescence intensity of each experimental plate and expressed them as a percentage. Samples were run in quadruplicates and deemed positive if at least two of the four replicates gave a fluorescence signal higher than the chosen threshold cut-off value, that was set as the 30% of the median of the maximum values reached by the positive control replicates during the 30-hour run.

Statistical analysis

Data are reported as mean, standard deviation, number, and percentage. We calculated sensitivity, specificity, positive predictive value, negative predictive value, and diagnostic accuracy, including 95% confidence intervals (CI), for the detection of α -synuclein in the skin and in the CSF by RT-QuIC

in patients with IRBD. In the skin, participants were categorized α -synuclein positive if at least one of the six skin samples were positive for α -synuclein by RT-QuIC. RT-QuIC fluorescence responses were analysed and plotted using GraphPad Prism 9.0 for Windows. Differences between groups were assessed using the χ^2 test and Fisher's exact test for categorical variables, and Student's t test and Mann-Whitney U test for continuous variables, as appropriate. We calculated the overall percentage agreement (the proportion of IRBD patients in whom the skin biopsy and the lumbar puncture gave the same positive or negative outcome for the presence of α -synuclein) between the skin biopsy and lumbar puncture results. All analyses were done with SPSS version 25.0 for Windows (SPSS, Inc., Chicago, IL). P values less than 0.05 were significant.

RESULTS

Mammana, Angela et al. "Detection of prions in skin punch biopsies of Creutzfeldt-Jakob disease patients."

Sample preparation and optimization of experimental conditions for skin prion RT-QuIC

In 2017, Orrù et colleagues detected for the first-time prion-seeding activity by RT-QuIC in post-mortem skin samples of 21 sCJD and 7 control patients with an overall sensitivity and specificity of 100%.¹⁸⁵ However, the protocol required a large punch biopsy (60 to 80 mg) and a time-consuming protocol for sample homogenization. In this perspective, we tried to adapt the protocol used for brain homogenate. Therefore, small pieces of skin punch (~25 mg) were homogenised at 1% in cold QuIC buffer (as described above), and after centrifugation, the supernatant was stored at -80°C. Based on the results obtained by Orrù et al., we decided to use the 10⁻³ dilution that gave the most effective reaction in terms of the distinction between positive and negative.¹⁸⁵

RT-QuIC assay: comparison between Ha23-231 and Bv23-230 recombinant prion protein

To evaluate the accuracy of RT-QuIC for the detection of prion seeding activity across the spectrum of human prion diseases, we compared the performance of two different recombinant substrates: Ha23-231 and Bv23-230. Orrù et al. demonstrated that the use of Bv23-230 recombinant prion protein as RT-QuIC substrate allows discrimination of prion strains such as classical and atypical L-type bovine spongiform encephalopathy, classical and atypical Nor98 scrapie in sheep as well as sporadic and variant Creutzfeldt-Jakob disease in humans,¹⁶⁹ as also demonstrated in skin samples.¹⁸⁵ Then, we wanted to evaluate if the use of this substrate, compared to Ha23-230, determine a higher accuracy in detecting PrP^{Sc} seeds in the skin across CJD subtypes. Although both protocols, in the neuropathological cohort, showed a 100% specificity in distinguishing CJD from non-CJD cases, the Bv23-230 demonstrated an overall better sensitivity (88.2% VS. 61.8% for Ha23-231), specifically in the CJDMM1, the most common sCJD subtype (85.0% VS. 40.0% for Ha23-231) (Table 5). In contrast, we found no difference for sCJDV2 and sCJDMV2K, which resulted in 100% sensitivity with both substrates. This result could be due to a higher prion seeding activity in these subtypes than in sCJDMM1.

Table 5. Results of the skin RT-QuIC assay in the neuropathological cohort using Ha23-231 or Bv 23-230 rec-PrP as substrate.

Neuropathological cohort	Ha23-231		Bv23-230	
	Cervical	Thigh	Cervical	Thigh
	Positive/tested (%)			
sCJD MM1	8/20 (40.0)	8/19 (42.1)	17/20 (85.0)	13/19 (68.4)
sCJD MM2	2/3 (66.7)	2/3 (66.7)	2/3 (66.7)	2/3 (66.7)
sCJD VV2	3/3 (100)	2/3 (66.7)	3/3 (100)	3/3 (100)
sCJD MV2K	2/2 (100)	2/2 (100)	2/2 (100)	2/2 (100)
gCJD:	3/3 (100)	2/3 (66.7)	3/3 (100)	3/3 (100)
-E200K-129M	2/2 (100)	2/2 (100)	2/2 (100)	2/2 (100)
-V210I-129M	1/1 (100)	0/1 (0.0)	1/1 (100)	1/1 (100)
non-CJD	0/19 (0.0)	0/18 (0.0)	0/19 (0.0)	0/18 (0.0)
Overall sensitivity	21/32 (65.6)		28/32 (87.5)	
Overall specificity	0/21 (100)		0/21 (100)	

sCJD: sporadic Creutzfeldt-Jakob disease; gCJD: genetic Creutzfeldt-Jakob disease

Additionally, as previously showed for CSF, gCJD with E200K mutation showed a slightly earlier and a statistically significant higher signal response than those of sCJDMM1, using both substrates (Bv, ThT max: gCJD-E200K 82963 ± 9927 vs. sCJDMM1 53570 ± 4611, p<0.05; Ha, ThT max: gCJD-E200K 238146 ± 4611 vs. sCJDMM1 9890 ± 11397, p=0.005 (Figure 7).

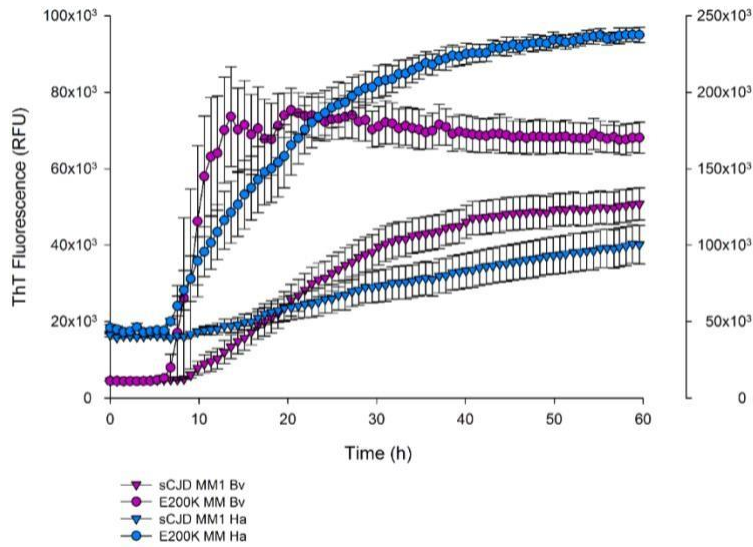


Figure 7. Comparison of skin RT-QuIC results in sCJDDMM1 and gCJD- E200K using Ha23-231 and Bv23-230. The gCJD-E200K skin samples showed a significant higher ThT fluorescence response than that from sCJMM1 cases using both Ha23-231 and Bv23-230 as substrate. Traces represents the mean of the ThT fluorescence expressed in RFU \pm SEM.

Comparison of prion seeding activity detection in skin and CSF samples from the same patient

CSF samples were available in 37 patients of the neuropathological cohort, which allowed us to compare the RT-QuIC results obtained with both CSF and skin; for the latter, we considered the results achieved using BV23-230 as substrate due to its higher sensibility compared with the Ha23-231. The results showed a very high concordance (34 of 37, 91.9%) (Table 6) between the positive and negative outcomes of the 2 assays. The 3 discordant cases are 2 sCJDDMM1 e one sCJDDMM2C case that showed a positive result in the CSF but not in the skin.

Table 6. Comparison of RT-QuIC sensitivity and specificity in skin and CSF of the same patient

Neuropathological cohort	Bv23-230	Ha90-231
	Skin overall	CSF
	Positive/tested (%)	
sCJD MM1	16/18 (88.9)	18/18 (100)
sCJD MM2	1/2 (50)	2/2 (100)
sCJD VV2	1/1 (100)	1/1 (100)
sCJD MV2K	2/2 (100)	2/2 (100)
gCJD:	3/3 (100)	3/3 (100)
-E200K-129M	2/2 (100)	2/2 (100)
-V210I-129M	1/1 (100)	1/1 (100)
non-CJD	0/21 (0.0)	0/11 (0.0)
Overall sensitivity	23/26 (88.5)	26/26 (100)
Overall specificity	0/21 (100)	0/11 (100)

RT-QuIC detection of prion in skin punch biopsies taken in vivo

After setting up skin RT-QuIC on a neuropathological cohort, we examined 5 patients who underwent in vivo skin biopsies of both cervical and thigh site. All samples gave a positive response in at least one of the two sites, using Bv23-230 substrate. In contrast, all non-CJD samples yielded a negative response, confirming the full specificity of the assay (Table 7). A positive fluorescence response was seen in four of five cervical samples, while one patient only showed positive result in the thigh. Only one of the four cases that were positive in the cervical site also gave a positive result in the thigh. Interestingly, ex vivo samples showed a significantly higher ThT max and a slightly shorter lag phase compared to the in vivo ones (ex vivo: 54861 ± 3440 vs. in vivo 33789 ± 7751 , $p < 0.05$) (Figure 8). The comparison of the RT-QuIC results of skin and CSF from the same patients, resulted in 100% concordance.

Table 7. RT-QuIC results of skin samples taken in vivo and CSF

In vivo	Ha23-231		Bv23-230		Ha90-231
	Cervical	Thigh	Cervical	Thigh	CSF
	Positive/tested (%)				
sCJD MM	½ (50.0)	0/2 (0)	2/2 (100)	0/2 (0)	2/2 (100)
sCJD MV	2/2 (100)	1/2 (50.0)	2/2 (100)	1/2 (50.0)	2/2 (100)
sCJD VV	0/1 (0)	1/1 (100)	0/1 (0)	1/1 (100)	1/1 (100)
non-CJD	0/10 (0)	0/12 (0)	0/10 (0)	0/12 (0)	0/6 (0.0)
Overall sensitivity	4/5 (80.0)		5/5 (100)		5/5 (100)
Overall specificity	0/12 (100)		0/12 (100)		0/1 (100)

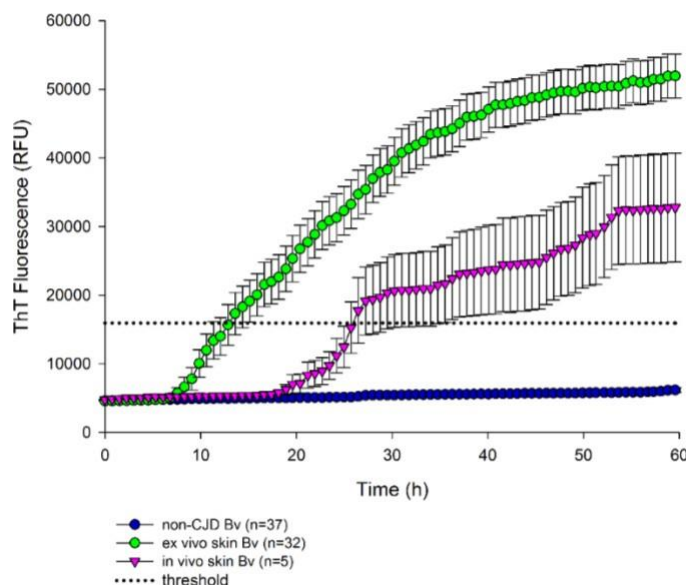


Figure 8. Comparison of kinetic curves of prion seeding activity of ex vivo and in vivo skin samples. Ex vivo skin samples (n=32) showed a significant higher fluorescence response and a slightly earlier lag phase than in vivo sample (n=5). Traces represent the mean of the ThT fluorescence expressed in RFU ± SEM.

Interestingly, two subjects underwent both in vivo and ex vivo punch biopsies; specifically, a sCJDMM1 patient who underwent in vivo skin biopsy one month from the clinical onset, gave a positive response in 3 out of 4 wells in the cervical and a negative outcome in the thigh. The corresponding ex vivo samples, taken 34 months later, gave full positivity in both areas with a significantly higher fluorescence response (ex vivo 113441 ± 15971 vs. in vivo 49810 ± 146144) and a shorter lag phase (ex vivo cervical 17.4 h vs. in vivo cervical 24.1 h) than the cervical skin samples taken in vivo (Figure 9 A). A sCJDMV2K patient underwent an in vivo skin biopsy 11.5 months from

the clinical onset and gave a partial positive response (3/4 wells) limited to the cervical area. The ex vivo sample, collected 1 month later, yielded an entirely positive outcome in both sites with a shorter lag phase in the cervical area (ex vivo 12.0 h vs. in vivo 19.6 h) but a similar maximum ThT response (Figure 9 B).

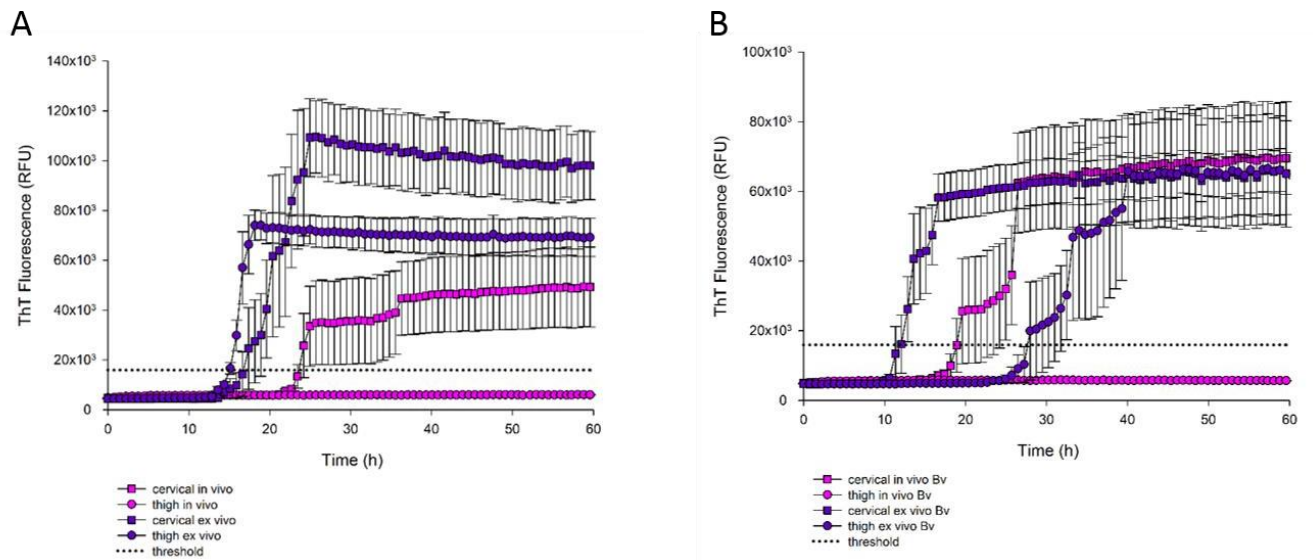


Figure 9. Comparison of RT-QuIC results of in vivo and ex vivo skin samples from the same patients. A) In a sCJDM1 case, both cervical and thigh ex vivo skin samples showed an earlier lag phase and a higher fluorescence response than the only in vivo skin sample tested positive. B) In a sCJDM2K case, both the ex vivo skin samples and the in vivo skin specimen from the cervical site tested positive with similar maximum ThT response, but different lag phase. Traces represent the mean of the ThT fluorescence expressed in RFU \pm SEM.

Mammana, Angela et al. “RT-QuIC Detection of Pathological α -Synuclein in Skin Punches of Patients with Lewy Body Disease”

Optimization of experimental conditions for skin α -Syn RT-QuIC

After the optimization of skin biopsy homogenization protocol in the previous study, we decided to use the same procedure, except for using PBS 1X as buffer, as this was the solution used for homogenization of brain samples for α -synuclein RT-QuIC.¹⁸⁰ Then, to evaluate the best condition for skin α -syn RT-QuIC, we tested various dilutions (w/v) of skin homogenates (from 10^{-2} to 10^{-4}). We used cervical samples from the postmortem cohort, including 4 LBD patients (1 PD, 1 DLB, and 2 incidental LBD) and 4 non-LBD controls. As shown in Figure 10, in all LBD samples tested, only the 10^{-2} dilution amplified the fluorescence signal consistently, providing the most effective reaction to distinguish positive from negative results. We, therefore, used this dilution to analyze all our samples.

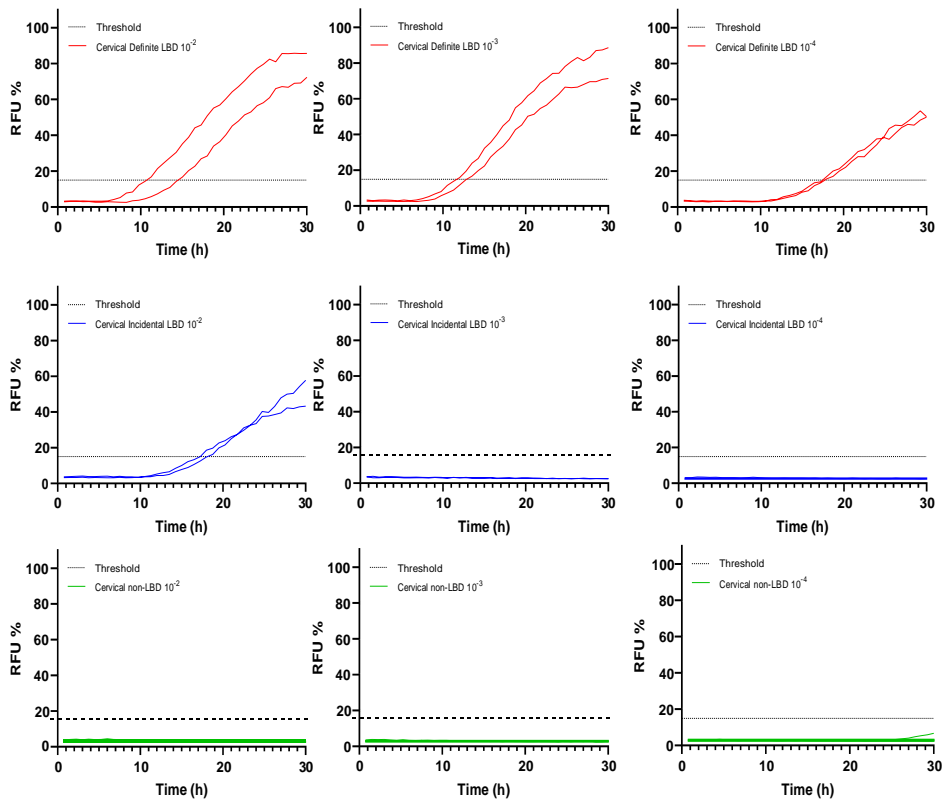


Figure 10. RT-QuIC endpoint dilution analysis of LBD and non-LBD skin homogenates from cervical samples. Serial dilutions (10^{-2} , 10^{-3} , and 10^{-4}) of skin homogenates from 2 definite LBD (top), 2 incidental LBD (middle), and 4 non-LBD patients (bottom) were tested. Each curve represents the average of the 4 replicates run for each sample.

RT-QuIC analysis of post-mortem skin punches for the detection of synuclein seeding activity

Among the 9 cervical samples from patients with neuropathologically confirmed LB pathology, 8 showed a 4/4 positive response (sensitivity, 88.9%), including one patient who only had focal LB pathology (Braak LB stage 1). In contrast, all but one of the non-LBD cervical samples yielded a negative response (specificity, 97.5%). Among the 8 patients who tested positive in the cervical site, 7 were also analyzed in the thigh, and 6 of 7 gave a positive response with fewer positive replicates in some cases (Figure 11, Table 8). DLB and PD patients, however, gave a full 4/4 positive response in both sites. Furthermore, all 39 non-LBD thigh samples were negative (Table 9).

Table 8. Neuropathological features and results of the α -syn RT-QuIC of the definite and incidental LBD group

List of cases	Sex	AAD	Primary NP diagnosis	Secondary NP diagnosis	Braak stage	RT-QuIC result ^b	
						Cervical	Thigh
Case #1	F	79	DLB	AD (intermediate)	6	4/4	4/4
Case #2	M	67	PD	AD (mild)	5	4/4	4/4
Case #3	M	76	DLB	AD (mild), CAA	4	4/4	2/4
Case #4 ^a	M	76	sCJD MM1 +2C	ILB pathology, AGD	3	4/4	3/4
Case #5	F	82	AD (intermediate)	ILB pathology, hippocampal sclerosis, LATE-NC, ARTAG	1	3/4	3/4
Case #6 ^a	F	64	sCJD MM1 + 2C	ILB pathology	3	4/4	0/4
Case #7 ^a	F	62	sCJD MM1	ILB pathology	3	4/4	2/4
Case #8	F	82	Primary CNS lymphoma	ILB pathology, PART	4	4/4	NA
Case #9	F	80	Cerebral ischemic stroke	Subcortical vascular encephalopathy, AD ^c (intermediate), ILB pathology	3	0/4	0/4

NP, neuropathologic; LB, Lewy bodies; RT-QuIC, real-time quaking-induced conversion; DLB, dementia with Lewy bodies; AD, Alzheimer's disease; PD, Parkinson's disease; VaE, Vascular Encephalopathy; CAA, cerebral amyloid angiopathy; ILB, incidental Lewy body; sCJD, sporadic Creutzfeldt-Jakob disease; AGD, argyrophilic grain disease; LATE-NC, Limbic-predominant age-related TDP-43 encephalopathy neuropathological change; ARTAG, aging-related tau astroglipathy; CNS, central nervous system; PART, primary age-related tauopathy. ^asCJD subtypes were defined in accordance with Parchi et al.²⁰² ^bNumber of positive replicates out of total tested replicates. ^cThe severity of AD neuropathologic change was assessed according to Montine et al. 2012.²⁰³

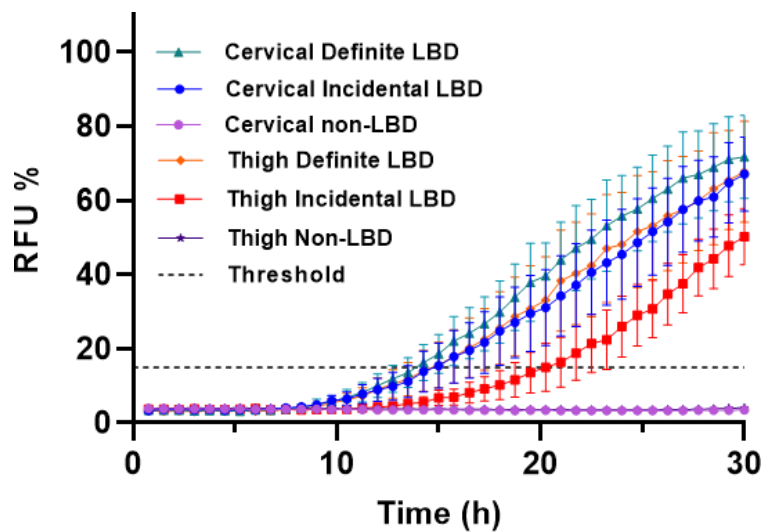


Figure 11. Kinetic curves of α -Syn seeding activity measured by RT-QuIC. Comparison among cervical and thigh skin homogenate seeding activity of neuropathologically confirmed LBD (n = 2 for both sites) and incidental LBD (cervical, n = 7; thigh, n = 6) and non-LBD (cervical, n = 40; thigh, n = 39) samples. Each curve represents the average of the analyzed group/site.

In addition, there was no significant difference in ThT max (Figure 12 A) and lag phase (Figure 12 B) between samples from the 2 examined sites.

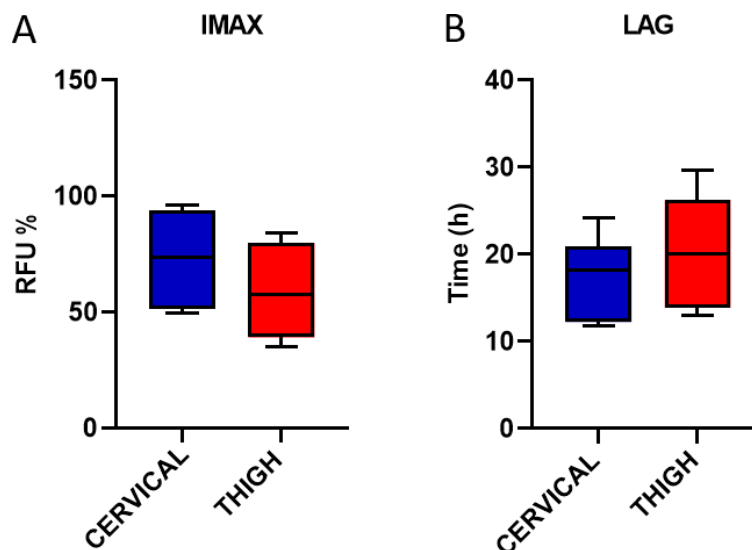


Figure 12. Analysis of kinetic parameters variations among cervical and thigh of ex vivo skin samples. Imax (A) and Lag phase (B) were investigated. No statistically significant differences were found between the two sites.

RT-QuIC analysis of *in vitam* skin biopsies for the detection of α -synuclein seeding activity

We subsequently evaluated the diagnostic value of skin RT-QuIC in a cohort of patients who underwent skin biopsy *in vitam*. Twenty-five of the 28 patients with probable LBD showed positive seeding activity (sensitivity, 89.3%), whereas 39 of 41 non-LBD tested negative (specificity, 95.1%; Table 9, Figure 13). Of the three skin samples of the LBD group tested RT-QuIC negative, two came from the thigh, and the third from the leg.

Table 9. Results of skin and CSF α -syn RT-QuIC

	<i>In vitam</i>			Post-mortem		
	DLB	PD	Controls	DLB, PD	iLBD	Non-LBD
RT-QuIC positive/tested (%)						
CSF	11/11 (100)	7/7 (100)	0/27 (0)	1/1 (100)	3/4 (75.0)	0/30 (0)
Skin Cervical	4/4 (100)	4/4 (100)	1/15 (6.7)	2/2 (100)	3/4 (75.0)	1/40 (2.5)
Skin Thigh	7/7 (100)	2/4 (50.0)	1/11 (9.1)	2/2 (100)	4/6 (66.7)	0/39 (0)
Skin Leg	4/4 (100)	4/5 (80.0)	0/15 (0)	-	-	-
Skin Overall*	15/15 (100)	10/13 (76.9)		2/2 (100)	6/7 (83.3)	
	25/28 (89.3)		2/41 (4.9)	8/9 (88.9)		1/40 (2.5)

*Patients examined postmortem were considered positive when at least 1 of the 2 sites showed α -synuclein seeding activity.

CSF, cerebrospinal fluid; DLB, dementia with Lewy bodies; iLBD, incidental Lewy body disease; PD, Parkinson's disease; RT-QuIC, real-time quaking-induced conversion.

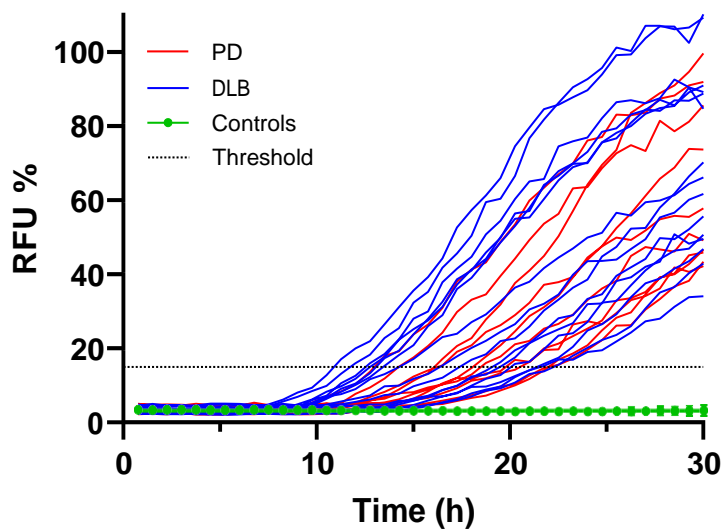


Figure 13. RT-QuIC detection of α -synuclein seeding activity in skin homogenates from the *in vitro* cohort patients. Each curve depicts the average of quadruplicates run for each LBD patient (PD, n = 13; DLB, n = 15). Non-LBD patients (n = 41) are represented as the average of the group.

There was no significant difference in the kinetics of the fluorescence response between PD and DLB patients (Figure 14).

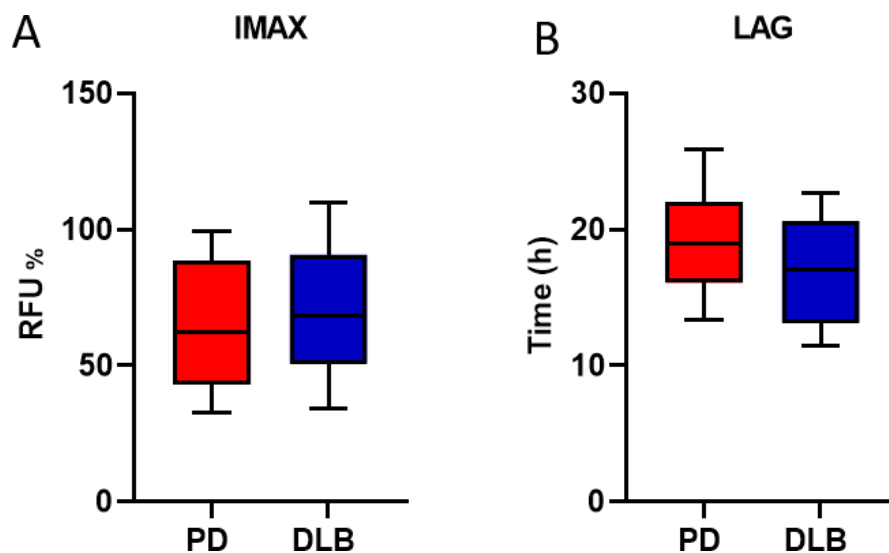


Figure 14. Analysis of kinetic parameters variations among PD and DLB cases. Imax (A) and Lag phase (B) were investigated. No statistically significant differences were found between the two sites.

The availability of a second punch for most of patients (26 LBD and 30 non-LBD controls), gave us the opportunity to validate the efficiency of the skin RT-QuIC assay. Results of skin RT-QuIC on the

second biopsy showed a 98.2% concordance with the first analysis in the positive/negative outcomes, including the negative results in 2 LBD patients not showing α -syn seeding activity in the first assay. Additionally, all LBD samples initially showing a positive reaction confirmed the result in the second assay. Interestingly, all but 2 positive samples gave a complete 4/4 response in both biopsies. Exceptions included 2 samples with 3/4 positive replicates, which in the second analysis gave 2/4 and 4/4. In the probable DLB group, only 1 biopsy from the thigh site showed a positive response (4/4) in the first analysis but no seeding activity in the second one.

Comparison of α -Synuclein seeding activity detection in skin and CSF samples from the same patient

CSF samples of 79 patients were available in addition to skin biopsies from both neuropathological and clinical cohorts. Therefore, we were able to compare the RT-QuIC results obtained using both biomatrices (Table 9). The results showed a very high concordance (76 of 79, 96.2%) between the 2 assays. The 3 discordant cases comprised 1 control from the *in vitam* cohort who was CSF negative but skin positive and 2 LBD patients from the postmortem cohort showing an inverse positive/negative discordance (1 skin positive but CSF negative and 1 skin negative but CSF positive). Additionally, we found no significant differences in the percentage of full (4/4) positive responses between the skin and CSF positive samples in both the postmortem ($P = 0.24$) and the *in vitam* ($P > 0.99$) cohorts.

Alex Iranzo, Angela Mammana, et al. "Misfolded α -synuclein assessment in skin and CSF by RT-QuIC in isolated REM sleep behaviour disorder"

RT-QuIC analysis of skin biopsies for the detection of synuclein seeding activity in iRBD patients

Since we had already validated the skin homogenization and dilution protocol for α -syn RT-QuIC in the previous work, we decided to also use the same protocol to detect the presence of α -synuclein aggregates in skin biopsies of patients with iRBD by RT-QuIC.

Skin biopsies from the 6 different sites were available for all 91 RBD patients. Skin α -syn RT-QuIC was positive in 70 of 91 patients and in 1 over the 41 controls resulting in a sensibility of 76.9% and specificity of 97.6%. The kinetics and overall results of skin α -syn RT-QuIC of patients and controls are shown in Figure 15 A-B.

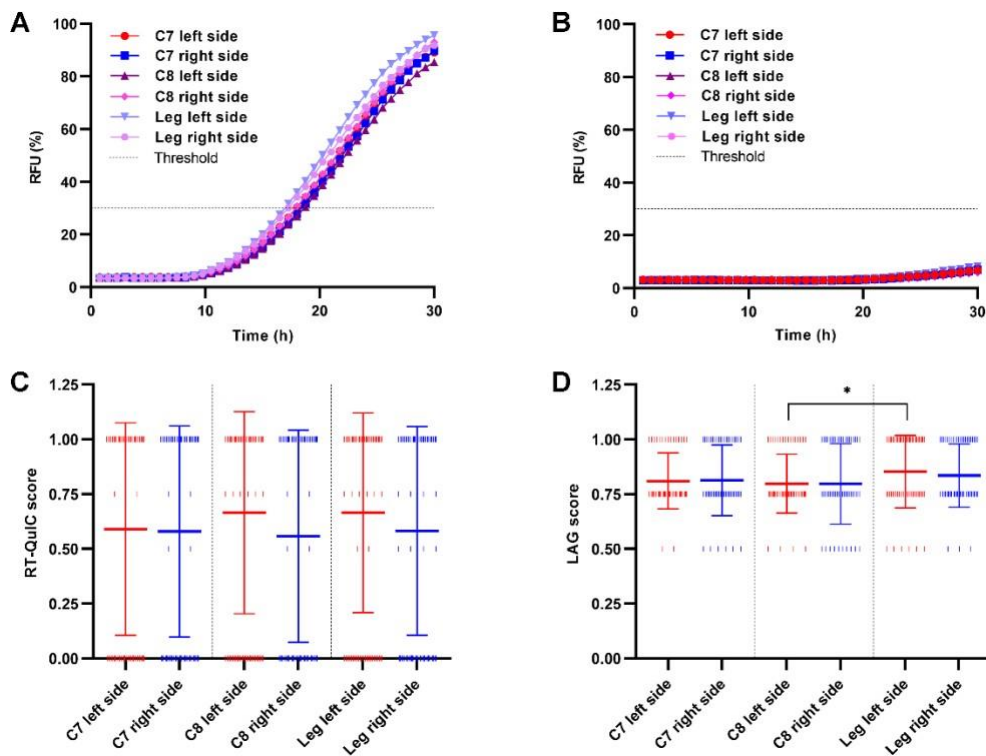


Figure 15. Kinetics of α -syn RT-QuIC reactions in the skin of IRBD patients. Mean normalized fluorescence emission for each skin site in IRBD patients (A) and controls (B). RFU= relative fluorescence units. Bars indicating the standard error of the mean were omitted to improve the readability. (C) Distribution in the number of RT-QuIC positive replicates among skin sites. We attributed an RT-QuIC score based on the number of positive wells and compared the score distribution among skin sites. D) Distribution of the LAG score across skin sites. Both leg sites showed a shorter LAG time than cervical sites, but only the difference between left C8 and left leg was significant ($*p \leq 0.05$). The RT-QuIC and LAG scores are plotted as mean \pm standard deviation. The vertical pipes indicate individual values. The red and blue lines in (C) and (D) indicate the skin site from the left and right sides, respectively. Panels (C) and (D) include only data from IRBD patients.

The analysis of all 6 sites highlighted the presence of differences in RT-QuIC response; specifically, of the 70 patients with a positive RT-QuIC result, left C7 was positive in 78.6% of the patients, right C7 in 78.6%, left C8 in 88.6%, right C8 in 75.7%, left distal leg in 90.0%, and right distal leg in 80.0%. However, most patients had α -synuclein seeding activity at multiple skin sites. Indeed, in 48.5% of the patients, α -synuclein was identified in all six sites, and 83% had at least four positive sites (Table 10). Two 3 sites combinations (left leg + right leg + left C7 and left leg + right leg + left C8) detected 100% α -synuclein skin positivity in the 70 α -synuclein positive patients. The number of patients with positivity in the cervical area were like those with positivity in the lower extremities (74.7% versus 75.8%; $p=0.86$). The cervical levels C7 and C8 (67.0% versus 72.5%; $p=0.42$) as well as the left and right sides, did not show any differences (72.5% vs 73.6%; $p=0.87$). The latter results were obtained after pooling the results from the C7, C8, and leg sites. Regarding the number of positive replicates, most positive skin samples gave a 4 of 4 response irrespectively to the site (Figure 15 C, Table 10). There were no significant differences in the kinetics of the fluorescence response measured by the

LAG time among most skin sites. The left leg site showed a significantly lower mean LAG time than the left C8 site as the only exception ($p=0.02$) (Figure 15)

Table 10. α -synuclein RT-QuIC results in skin and cerebrospinal fluid of patients and controls

Skin α -syn RT-QuIC single site results	Positive / tested (%)	Positive replicates (%)			LAG time (mean \pm SD)		
		4/4	3/4	2/4			
C7 left side	55/91 (60.4)	90.9	5.5	3.6	19.4 \pm 2.9		
C7 right side	55/91 (60.4)	89.9	5.5	5.5	19.8 \pm 3.5		
C8 left side	62/91 (68.1)	90.3	9.7	0	20.0 \pm 3.3		
C8 right side	53/91 (58.2)	88.7	3.8	7.5	19.5 \pm 3.6		
Leg left side	63/91 (69.2)	87.3	9.5	3.2	18.4 \pm 3.4		
Leg right side	56/91 (61.5)	85.7	7.1	7.1	18.4 \pm 3.0		
CSF AS RT-QuIC results	66/88 (75.0)	65.2	25.8	9.0	19.2 \pm 3.0		
Skin α-syn RT-QuIC combined site results		+ Best third site			Positive / tested (%)		
Left C7 + Left leg	68/91 (74.7)	+ Right leg			70/91 (76.9)		
Left C7 + Right leg	65/91 (71.4)	+ Left leg			70/91 (76.9)		
Left C8 + Right leg	65/91 (71.4)	+ Left leg			70/91 (76.9)		
Left leg + Right leg	69/91 (75.8)	+ Left C7			70/91 (76.9)		
Positive skin sites per subject, n/n	6/6	5/6	4/6	3/6	2/6	1/6	0/6
IRBD total (n=91), %	37.3	19.8	7.7	3.3	5.5	3.3	23.1
α -syn RT-QuIC positive IRBD (n=70), %	48.5	25.7	10.0	4.3	7.2	4.3	-
Controls (n=41), %	2.4	-	-	-	-	-	97.6

Comparison of α -Synuclein seeding activity detection in skin and CSF samples from the same patient

Then we compared the efficiency RT-QuIC to identify the presence of α -synuclein aggregates in the skin and CSF.

In the CSF, RT-QuIC was α -synuclein positive in 66 (75.0%) of 88 patients and in one (2.5%) of 40 controls, giving a sensitivity of 75.0% (95% CI 64.6–83.6), specificity of 97.5% (95% CI 86.8–99.9) and accuracy of 82.0% (95% CI 74.3–88.3). A comparison of the RT-QuIC kinetics curves between skin and CSF positive samples is shown in Figure 16 A.

128 participants (88 patients plus 40 controls) underwent both procedures. Among the 88 patients, 67 (52.3%) were α -synuclein positive in both skin and CSF, one (0.8%) was positive in the skin but negative in CSF, and none (0%) was negative in the skin but positive in CSF. Among the 40 controls,

only one (2.5%) was α -syn RT-QuIC positive in both skin and CSF. In these 128 participants, the overall agreement between α -syn RT-QuIC result in the skin and CSF was 99.2%. In the 88 iRBD patients, the agreement was 98.9%. In controls, the agreement was 100%. In the overall cohort, CSF had a significantly higher percentage of positive RT-QuIC reactions (75%) than individual skin sites (left C7 60.4%, $p=0.04$; right C7 60.4%, $p=0.04$; left C8 68.1%, $p=0.31$; right C8 58.2%, $p=0.02$; left distal leg 69.2%, $p=0.39$; right distal leg 61.5%, $p=0.05$) (Table 10). The skin samples, however, showed a higher prevalence of 4 of 4 positive replicates than the CSF samples (Table 10), suggesting that the apparent discrepancy could be caused by an uneven distribution of α -Synuclein aggregates. We calculated an RT-QuIC score that accounts for both the number of positive replicates in positive samples and the number of negative samples in each individual who tested positive by RT-QuIC (Figure 16 B). Applying this score, we found no difference between skin and CSF, a result in line with the similar LAG time detected in CSF and skin samples (Figure 16 B).

Patients were contacted one week after LP and skin biopsy to assess adverse effects. No severe or moderate adverse effects were reported. One hundred and ten (83.3%) participants stated that they would accept to undergo again another skin biopsy in the future, and 103 (80.5%) would accept to undergo again another lumbar puncture in the future.

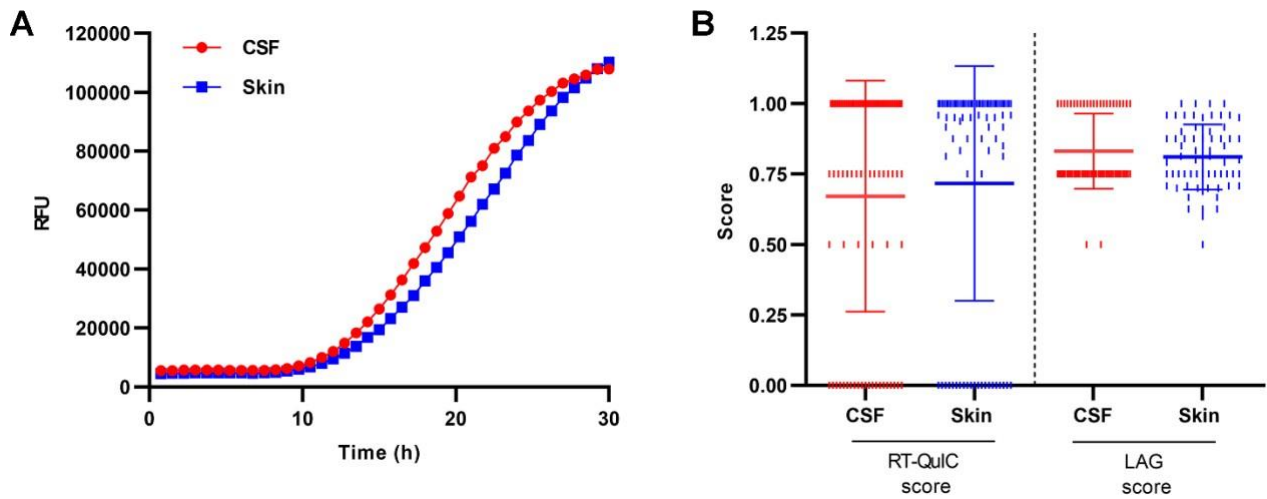


Figure 16. Comparison of α -synuclein seeding activity in skin and CSF of iRBD patients. A) Comparison of α -syn RT-QuIC kinetics of fluorescence emission between skin (mean of all positive sites) and CSF. RFU= relative fluorescence units. Bars indicating the standard error of the mean were omitted to improve the readability. B) Comparison of the number of positive replicates (RT-QuIC score, left) and LAG times (LAG score, right) between the skin (mean of all positive sites) and CSF. Only participants with CSF and at least one RT-QuIC positive skin site were evaluated (n=87). The RT-QuIC and LAG scores are plotted as mean \pm standard deviation. The vertical pipes indicate individual values.

DISCUSSION AND CONCLUSIONS

In recent years, the setup of RT-QuIC and other seeding amyloid assays (SAA) provided a critical advance in the diagnostic accuracy of Creutzfeldt-Jakob disease,^{156,164,209} and later also for other prion-like disorders, including PD and DLB.^{178,180,181}

CSF is the matrix of choice for RT-QuIC due to its high performance and accessibility as a fluid proximal to the brain, where protein aggregates predominantly accumulate. Additionally, CSF is routinely collected in patients with RPD for diagnostic purposes. However, the established presence of PrP^{Sc}^{182–184} and α -synuclein^{207,211} aggregates in peripheral tissues prompted the investigation of their potential use as an alternative to CSF for the diagnosis of both prion diseases and LBD. Along this line, we focused our interest on the use of skin punch biopsy as a potential biomatrix for RT-QuIC.

In 2017, Orrù and colleagues detected for the first time PrP^{Sc} aggregates in post-mortem skin punch biopsies by RT-QuIC with an overall sensibility and specificity of 100%.¹⁸⁵ Given the availability at the Laboratory of Neuropathology at ISNB of several skin punches from neuropathologically confirmed CJD patients and non-CJD and an established protocol for prion RT-QuIC, we decided to test our samples and compare the results of skin RT-QuIC with the CSF analysis. First, we tried to improve the method of sample preparation using a limited amount of tissue and the least time-consuming protocol. Then, we compared the efficiency of two different substrates to detect PrP^{Sc} aggregates by RT-QuIC: Ha23-231 and Bv23-230. In a neuropathologically confirmed cohort of 32 CJD and 21 non-CJD patients, we obtained a 100% specificity with both substrates and a higher sensitivity of Bv23-230 compared to the Ha23-231 PrP recombinant substrate (87.5% vs. 65.6%, respectively).

Interestingly, the lower performance of the PrP Ha substrate with samples from the MM1 sCJD subtype is consistent with previous findings of our group, demonstrating a lower PrP^{Sc} seeding activity in peripheral tissues in the M1 CJD strain compared with the V2 strain.¹⁸⁶

Consequently, we speculated that a higher PrP^{Sc} deposition characterizes the skin of sCJDV2 and sCJDMV2K patients, compared to the MM1, since also the Ha23-230 could detect PrP^{Sc} seeding activity in all these cases. Then, since 41 patients underwent both skin biopsy and LP, we could compare the performance of skin and CSF prion RT-QuIC. The results showed high concordance between the two protocols (38/41, 92.7%). This agreement was also demonstrated in a small cohort of patients who underwent skin biopsy *in vitam* since both assays identified PrP^{Sc} seeding activity in all the 5 patients analyzed and in none of the controls. Interestingly, of 2 of these patients, we had

both the *in vitam* and the *ex vivo* skin punch biopsies. The results from these samples, which showed a limited positive response in the cervical taken in *vitam*, as well as in the CSF, and a completely positive response in both the cervical and thigh in the *ex vivo* samples, suggest that prion seeding activity in the skin increases over time with disease progression.

The shared prion-like mechanism of protein aggregates formation and spread between prion protein and alpha-synuclein led some groups to adapt the RT-QuIC protocol for analyzing alpha-synuclein seeding activity.^{178,210} Indeed, in recent years, many studies successfully demonstrated the promising use of α -syn RT-QuIC in diagnosing all LB-related synucleinopathies.^{180,181} The presence of α -synuclein aggregates in the skin of patients affected by LBD is well known, and it was mainly demonstrated by immunohistochemical studies.²⁰⁷ After the optimization of α -syn RT-QuIC, two different groups also demonstrated the presence of α -synuclein seeding activity in a neuropathologically confirmed population¹⁹⁵ and a small cohort of living patients affected by Parkinson's disease.¹⁹⁴ Following this evidence, we used the α -syn RT-QuIC protocol used in our lab and a house-made K23Q as the substrate to evaluate the efficiency of the assay to detect α -synuclein seeds in skin punches from patients with PD, DLB, and incidental LB pathology. Skin α -syn RT-QuIC showed a sensibility of 88.9% in the neuropathologically confirmed LBD patients and a 97.5% specificity. Interestingly, this study showed an earlier negative response in more diluted samples of 7 patients with incidental LBD pathology and a relatively low Braak stage²⁰⁵ compared to PD and DLB samples, suggesting a lower α -synuclein seeding activity reflecting the focal CNS LB pathology in these samples.

Then, we investigated a clinical cohort of LBD patients who underwent a skin biopsy in *vitam*. In this cohort, α -syn RT-QuIC demonstrated a sensitivity of 89.3 % and specificity of 95.1 % (95% CI, 83.9%-97.6%). The availability of only one punch per patient limited the comparison between different skin sites. However, the higher sensitivity obtained in the cervical samples, the finding that all 3 RT-QuIC negative patients with clinical PD were analyzed in distal locations (thigh or leg), and the detection of a trend toward higher fluorescence reactivity in cervical samples favor the cervical area as the most suitable site for skin RT-QuIC.

As in the previous work,¹⁹⁹ we directly compare the performance of skin and CSF α -syn RT-QuIC. The two protocols showed a high agreement in sensitivity and specificity (76 of 79, 96.2%), confirming skin use as an alternative to CSF for the RT-QuIC assay. The slight difference between the two protocols can be mainly attributable to the small number of samples available for this sub analysis.

Different groups demonstrated the ability of RT-QuIC to detect α -synuclein seeding activity in patients' CSF in the prodromal phase of the synucleinopathies, including iRBD.^{181,212} Then, in collaboration with Dr. Iranzo, we evaluated the efficiency of RT-QuIC in detecting α -synuclein seeding activity in the skin of a cohort of 91 iRBD patients. Among the 91 iRBD tested, RT-QuIC showed a sensibility of 76.9% and specificity of 97.6% in the 41 controls. Six sites were analyzed from each patient, and 100% skin α -synuclein positivity was detected by combining only three sites (both distal legs plus left C7 or C8). Our results also suggested no difference between the proximal and distal sites and the right and left sides. Despite this evidence, multicentre studies with larger cohorts are required to identify the more suitable anatomical site for iRBD patients. For 88 patients, both skin and CSF were available. We found that RT-QuIC identified α -synuclein with similar high sensitivity and accuracy in the skin as in the CSF, with an agreement of 99% between the two protocols. These promising results suggested that α -syn RT-QuIC in either CSF or skin is a highly sensitive and specific biomarker of the prodromal stage of the synucleinopathies that could be used for patient stratification in future neuroprotective trials in iRBD. However, because our α -syn RT-QuIC protocol cannot detect α -synuclein aggregates in MSA, some iRBD patients who will develop MSA may not be included.

Along with skin RT-QuIC, many groups try to adapt the prion and α -syn RT-QuIC assays to other accessible peripheral tissues.^{163,189,191,192,196–198} The olfactory mucosa has attracted particular attention because the procedure of nasal brushing is easy and less aggressive than the lumbar puncture and skin biopsy and does not require anesthesia. Additionally, it can be obtained in individuals taking anticoagulants. Regarding prion diseases, RT-QuIC of olfactory mucosa showed a high sensitivity ranging from 95% to 100% and a 100% specificity, demonstrating the high diagnostic performance of this test.^{154,163}

Several studies investigated the presence of α -synuclein seeding activity in DLB and iRBD patients. In DLB, the sensitivity of the assay ranged from 55% to 84 %, and the specificity was around 90%.^{191,192,198,213} In one study in iRBD, sensitivity to detect α -synuclein in the olfactory mucosa was 44%, and specificity was 90%.²¹⁴

Based on these results, skin RT-QuIC has comparable accuracy to prion RT-QuIC on olfactory mucosa and higher diagnostic value for both DLB and iRBD populations.

In conclusion, our studies indicate that skin is a promising biomatrix for the early detection of misfolded proteins by RT-QuIC in neurodegenerative diseases, with a diagnostic value comparable to CSF RT-QuIC. A skin biopsy may be preferable to a lumbar puncture because it is a minimally

invasive technique associated with minor discomfort and complications; the procedure is quick, easy to perform, well tolerated, inexpensive, and requires no sutures. However, further studies are needed to confirm these findings, establish a shared protocol for skin sample preparation, and define the most suitable skin site for RT-QulC analysis.

BIBLIOGRAPHY

1. Dugger, B. N. & Dickson, D. W. Pathology of Neurodegenerative Diseases. *Cold Spring Harb. Perspect. Biol.* **9**, a028035 (2017).
2. Block, A. J. & Bartz, J. C. Prion strains: shining new light on old concepts. *Cell Tissue Res.* (2022) doi:10.1007/s00441-022-03665-2.
3. Creutzfeldt, H. G. On a particular focal disease of the central nervous system (preliminary communication). *Alzheimer Assoc Disord* **3**, 3–25.
4. Jakob, A. M. Über eine eigenartige herdförmige Erkrankung des Zentralnervensystems. *Z Ges Neurol Psychiatry* **70**, 132–146.
5. Prusiner, S. B. Novel Proteinaceous Infectious Particles Cause Scrapie. *Science* **216**, 136–144 (1982).
6. Bolton, D. C., McKinley, M. P. & Prusiner, S. B. Identification of a Protein That Purifies with the Scrapie Prion. *Science* **218**, 1309–1311 (1982).
7. Basler, K. *et al.* Scrapie and cellular PrP isoforms are encoded by the same chromosomal gene. *Cell* **46**, 417–428 (1986).
8. Puckett, C., Concannon, P., Casey, C. & Hood, L. Genomic structure of the human prion protein gene. *Am. J. Hum. Genet.* **49**, 320–329 (1991).
9. Kretzschmar, H. A. *et al.* Molecular Cloning of a Human Prion Protein cDNA. *DNA* **5**, 315–324 (1986).
10. Stahl, N., Baldwin, M. A., Burlingame, A. L. & Prusiner, S. B. Identification of glycoinositol phospholipid-linked and truncated forms of the scrapie prion protein. *Biochemistry* **29**, 8879–8884 (1990).
11. Endo, T., Groth, D., Prusiner, S. B. & Kobata, A. Diversity of oligosaccharide structures linked to asparagines of the scrapie prion protein. *Biochemistry* **28**, 8380–8388 (1989).
12. Shyng, S. L., Heuser, J. E. & Harris, D. A. A glycolipid-anchored prion protein is endocytosed via clathrin-coated pits. *J. Cell Biol.* **125**, 1239–1250 (1994).

13. Aguzzi, A., Sigurdson, C. & Heikenwaelder, M. Molecular Mechanisms of Prion Pathogenesis. *Annu. Rev. Pathol. Mech. Dis.* **3**, 11–40 (2008).
14. Sunyach, C. The mechanism of internalization of glycosylphosphatidylinositol-anchored prion protein. *EMBO J.* **22**, 3591–3601 (2003).
15. Yim, Y.-I. *et al.* The multivesicular body is the major internal site of prion conversion. *J. Cell Sci.* **128**, 1434–1443 (2015).
16. Guo, B. B., Bellingham, S. A. & Hill, A. F. The Neutral Sphingomyelinase Pathway Regulates Packaging of the Prion Protein into Exosomes. *J. Biol. Chem.* **290**, 3455–3467 (2015).
17. Brown, D. R., Clive, C. & Haswell, S. J. Antioxidant activity related to copper binding of native prion protein: SOD and PrP. *J. Neurochem.* **76**, 69–76 (2008).
18. Petit, C. S. V., Besnier, L., Morel, E., Rousset, M. & Thenet, S. Roles of the cellular prion protein in the regulation of cell-cell junctions and barrier function. *Tissue Barriers* **1**, e24377 (2013).
19. Peggion, C., Bertoli, A. & Sorgato, M. C. Almost a century of prion protein(s): From pathology to physiology, and back to pathology. *Biochem. Biophys. Res. Commun.* **483**, 1148–1155 (2017).
20. Sweeney, P. *et al.* Protein misfolding in neurodegenerative diseases: implications and strategies. *Transl. Neurodegener.* **6**, 6 (2017).
21. Cox, B., Ness, F. & Tuite, M. Analysis of the Generation and Segregation of Propagons: Entities That Propagate the [PSI⁺] Prion in Yeast. *Genetics* **165**, 23–33 (2003).
22. Scheckel, C. & Aguzzi, A. Prions, prionoids and protein misfolding disorders. *Nat. Rev. Genet.* **19**, 405–418 (2018).
23. Soto, C. & Satani, N. The intricate mechanisms of neurodegeneration in prion diseases. *Trends Mol. Med.* **17**, 14–24 (2011).
24. Hetz, C. & Mollereau, B. Disturbance of endoplasmic reticulum proteostasis in neurodegenerative diseases. *Nat. Rev. Neurosci.* **15**, 233–249 (2014).

25. Torres, M. *et al.* ER stress signaling and neurodegeneration: At the intersection between Alzheimer's disease and Prion-related disorders. *Virus Res.* **207**, 69–75 (2015).
26. Chiesa, R. The Elusive Role of the Prion Protein and the Mechanism of Toxicity in Prion Disease. *PLOS Pathog.* **11**, e1004745 (2015).
27. Parchi, P., Strammiello, R., Giese, A. & Kretzschmar, H. Phenotypic variability of sporadic human prion disease and its molecular basis: past, present, and future. *Acta Neuropathol. (Berl.)* **121**, 91–112 (2011).
28. Masters, c. L. & Richardson, E. P. SUBACUTE SPONGIFORM ENCEPHALOPATHY (CREUTZFELDT-JAKOB DISEASE): THE NATURE AND PROGRESSION OF SPONGIFORM CHANGE. *Brain* **101**, 333–344 (1978).
29. Palmer, M. S., Dryden, A. J., Hughes, J. T. & Collinge, J. Homozygous prion protein genotype predisposes to sporadic Creutzfeldt–Jakob disease. *Nature* **352**, 340–342 (1991).
30. Hsiao, K. *et al.* Mutant prion proteins in Gerstmann-Sträussler-Scheinker disease with neurofibrillary tangles. *Nat. Genet.* **1**, 68–71 (1992).
31. Petersen, R. B. *et al.* Analysis of the prion protein gene in thalamic dementia. *Neurology* **42**, 1859–1859 (1992).
32. Capellari, S., Strammiello, R., Saverioni, D., Kretzschmar, H. & Parchi, P. Genetic Creutzfeldt–Jakob disease and fatal familial insomnia: insights into phenotypic variability and disease pathogenesis. *Acta Neuropathol. (Berl.)* **121**, 21–37 (2011).
33. Chapman, J., Ben-Israel, J., Goldhammer, Y. & Korczyn, A. D. The risk of developing Creutzfeldt-Jakob disease in subjects with the PRNP gene codon 200 point mutation. *Neurology* **44**, 1683–1683 (1994).
34. D'Alessandro, M., Petraroli, R., Ladogana, A. & Pocchiari, M. High incidence of Creutzfeldt-Jakob disease in rural Calabria, Italy. *The Lancet* **352**, 1989–1990 (1998).

35. Goldfarb, LevG., Mitrová, E., Brown, P., Hock Toh, B. & Carleton Gajdusek, D. Mutation in codon 200 of scrapie amyloid protein gene in two clusters of Creutzfeldt-Jakob disease in Slovakia. *The Lancet* **336**, 514–515 (1990).
36. Ladogana, A. *et al.* High incidence of genetic human transmissible spongiform encephalopathies in Italy. *Neurology* **64**, 1592–1597 (2005).
37. Foliaki, S. *et al.* Pathogenic Prion Protein Isoforms Are Not Present in Cerebral Organoids Generated from Asymptomatic Donors Carrying the E200K Mutation Associated with Familial Prion Disease. *Pathogens* **9**, 482 (2020).
38. Takada, L. & Geschwind, M. Prion Diseases. *Semin. Neurol.* **33**, 348–356 (2013).
39. Parchi, P. *et al.* Classification of sporadic Creutzfeldt-Jakob disease based on molecular and phenotypic analysis of 300 subjects. *Ann. Neurol.* **46**, 224–233 (1999).
40. Parchi, P. *et al.* Typing prion isoforms. *Nature* **386**, 232–233 (1997).
41. Parchi, P. *et al.* Molecular basis of phenotypic variability in sporadic creudeldt-jakob disease. *Ann. Neurol.* **39**, 767–778 (1996).
42. Parchi, P. *et al.* Genetic influence on the structural variations of the abnormal prion protein. *Proc. Natl. Acad. Sci.* **97**, 10168–10172 (2000).
43. Parchi, P. *et al.* Incidence and spectrum of sporadic Creutzfeldt–Jakob disease variants with mixed phenotype and co-occurrence of PrPSc types: an updated classification. *Acta Neuropathol. (Berl.)* **118**, 659–671 (2009).
44. Parchi, P. *et al.* Different patterns of truncated prion protein fragments correlate with distinct phenotypes in P102L Gerstmann–Sträussler–Scheinker disease. *Proc. Natl. Acad. Sci.* **95**, 8322–8327 (1998).
45. Jansen, C. *et al.* The first case of protease-sensitive prionopathy (PSP_{Pr}) in The Netherlands: a patient with an unusual GSS-like clinical phenotype. *J. Neurol. Neurosurg. Psychiatry* **81**, 1052–1055 (2010).

46. Cronier, S., Laude, H. & Peyrin, J.-M. Prions can infect primary cultured neurons and astrocytes and promote neuronal cell death. *Proc. Natl. Acad. Sci.* **101**, 12271–12276 (2004).
47. Cronier, S. *et al.* Endogenous prion protein conversion is required for prion-induced neuritic alterations and neuronal death. *FASEB J.* **26**, 3854–3861 (2012).
48. Zhu, C. *et al.* A neuroprotective role for microglia in prion diseases. *J. Exp. Med.* **213**, 1047–1059 (2016).
49. McCulloch, L. *et al.* Follicular Dendritic Cell-Specific Prion Protein (PrP_c) Expression Alone Is Sufficient to Sustain Prion Infection in the Spleen. *PLoS Pathog.* **7**, e1002402 (2011).
50. Kanu, N. *et al.* Transfer of Scrapie Prion Infectivity by Cell Contact in Culture. *Curr. Biol.* **12**, 523–530 (2002).
51. Gousset, K. *et al.* Prions hijack tunnelling nanotubes for intercellular spread. *Nat. Cell Biol.* **11**, 328–336 (2009).
52. Zhu, S., Victoria, G. S., Marzo, L., Ghosh, R. & Zurzolo, C. Prion aggregates transfer through tunneling nanotubes in endocytic vesicles. *Prion* **9**, 125–135 (2015).
53. Victoria, G. S., Arkhipenko, A., Zhu, S., Syan, S. & Zurzolo, C. Astrocyte-to-neuron intercellular prion transfer is mediated by cell-cell contact. *Sci. Rep.* **6**, 20762 (2016).
54. Arellano-Anaya, Z. E. *et al.* Prion strains are differentially released through the exosomal pathway. *Cell. Mol. Life Sci.* **72**, 1185–1196 (2015).
55. Sigurdson, C. J., Bartz, J. C. & Glatzel, M. Cellular and Molecular Mechanisms of Prion Disease. *Annu. Rev. Pathol. Mech. Dis.* **14**, 497–516 (2019).
56. McBride, P. A. *et al.* Early Spread of Scrapie from the Gastrointestinal Tract to the Central Nervous System Involves Autonomic Fibers of the Splanchnic and Vagus Nerves. *J. Virol.* **75**, 9320–9327 (2001).
57. Fraser, H. Neuronal spread of scrapie agent and targeting of lesions within the retino-tectal pathway. *Nature* **295**, 149–150 (1982).

58. Bett, C. *et al.* Biochemical Properties of Highly Neuroinvasive Prion Strains. *PLoS Pathog.* **8**, e1002522 (2012).
59. Bett, C. *et al.* Defining the Conformational Features of Anchorless, Poorly Neuroinvasive Prions. *PLoS Pathog.* **9**, e1003280 (2013).
60. Aguilar-Calvo, P. *et al.* Generation of novel neuroinvasive prions following intravenous challenge: Prion Strain Mutation After an IV Exposure. *Brain Pathol.* **28**, 999–1011 (2018).
61. Takatsuki, H. *et al.* Prion-Seeding Activity Is widely Distributed in Tissues of Sporadic Creutzfeldt-Jakob Disease Patients. *EBioMedicine* **12**, 150–155 (2016).
62. Glatzel, M., Abela, E., Maissen, M. & Aguzzi, A. Extraneural Pathologic Prion Protein in Sporadic Creutzfeldt–Jakob Disease. *N. Engl. J. Med.* **349**, 1812–1820 (2003).
63. Rubenstein, R. & Chang, B. Re-Assessment of PrPSc Distribution in Sporadic and Variant CJD. *PLoS ONE* **8**, e66352 (2013).
64. Glatzel, M., Giger, O., Braun, N. & Aguzzi, A. The Peripheral Nervous System and the Pathogenesis of Prion Diseases. *Curr. Mol. Med.* **4**, 355–359 (2004).
65. Orrú, C. D. *et al.* Prion seeding activity and infectivity in skin samples from patients with sporadic Creutzfeldt-Jakob disease. *Sci. Transl. Med.* **9**, eaam7785 (2017).
66. Baiardi, S. *et al.* Prion-related peripheral neuropathy in sporadic Creutzfeldt-Jakob disease. *J. Neurol. Neurosurg. Psychiatry* **90**, 424–427 (2019).
67. Maroteaux, L., Campanelli, J. & Scheller, R. Synuclein: a neuron-specific protein localized to the nucleus and presynaptic nerve terminal. *J. Neurosci.* **8**, 2804–2815 (1988).
68. Gonçalves, S. & Outeiro, T. F. Assessing the Subcellular Dynamics of Alpha-synuclein Using Photoactivation Microscopy. *Mol. Neurobiol.* **47**, 1081–1092 (2013).
69. McLean, P. J., Ribich, S. & Hyman, B. T. Subcellular localization of α -synuclein in primary neuronal cultures: effect of missense mutations. in *Advances in Research on Neurodegeneration* (eds. Mizuno, Y. *et al.*) 53–63 (Springer Vienna, 2000). doi:10.1007/978-3-7091-6284-2_5.

70. Mori, F., Tanji, K., Yoshimoto, M., Takahashi, H. & Wakabayashi, K. Demonstration of α -Synuclein Immunoreactivity in Neuronal and Glial Cytoplasm in Normal Human Brain Tissue Using Proteinase K and Formic Acid Pretreatment. *Exp. Neurol.* **176**, 98–104 (2002).
71. Uéda, K. *et al.* Molecular cloning of cDNA encoding an unrecognized component of amyloid in Alzheimer disease. *Proc. Natl. Acad. Sci.* **90**, 11282–11286 (1993).
72. Nakajo, S. *et al.* Purification and Characterization of a Novel Brain-Specific 14-kDa Protein. *J. Neurochem.* **55**, 2031–2038 (1990).
73. Jakes, R., Spillantini, M. G. & Goedert, M. Identification of two distinct synucleins from human brain. *FEBS Lett.* **345**, 27–32 (1994).
74. Bruening, W. *et al.* Synucleins are expressed in the majority of breast and ovarian carcinomas and in preneoplastic lesions of the ovary. *Cancer* **88**, 2154–2163 (2000).
75. Polymeropoulos, M. H. *et al.* Mutation in the α -Synuclein Gene Identified in Families with Parkinson's Disease. *Science* **276**, 2045–2047 (1997).
76. Lee, V. M.-Y. & Trojanowski, J. Q. Mechanisms of Parkinson's Disease Linked to Pathological α -Synuclein: New Targets for Drug Discovery. *Neuron* **52**, 33–38 (2006).
77. George, J. M., Jin, H., Woods, W. S. & Clayton, D. F. Characterization of a novel protein regulated during the critical period for song learning in the zebra finch. *Neuron* **15**, 361–372 (1995).
78. Sode, K., Ochiai, S., Kobayashi, N. & Usuzaka, E. Effect of Reparation of Repeat Sequences in the Human α -Synuclein on Fibrillation Ability. *Int. J. Biol. Sci.* 1–7 (2007) doi:10.7150/ijbs.3.1.
79. Burré, J., Sharma, M. & Südhof, T. C. Cell Biology and Pathophysiology of α -Synuclein. *Cold Spring Harb. Perspect. Med.* **8**, a024091 (2018).
80. Bell, R. & Vendruscolo, M. Modulation of the Interactions Between α -Synuclein and Lipid Membranes by Post-translational Modifications. *Front. Neurol.* **12**, 661117 (2021).
81. Bartels, T., Choi, J. G. & Selkoe, D. J. α -Synuclein occurs physiologically as a helically folded tetramer that resists aggregation. *Nature* **477**, 107–110 (2011).

82. Wang, W. *et al.* A soluble α -synuclein construct forms a dynamic tetramer. *Proc. Natl. Acad. Sci.* **108**, 17797–17802 (2011).
83. Davidson, W. S., Jonas, A., Clayton, D. F. & George, J. M. Stabilization of α -Synuclein Secondary Structure upon Binding to Synthetic Membranes. *J. Biol. Chem.* **273**, 9443–9449 (1998).
84. Iwai, A. *et al.* The precursor protein of non-A β component of Alzheimer's disease amyloid is a presynaptic protein of the central nervous system. *Neuron* **14**, 467–475 (1995).
85. Kahle, P. J. *et al.* Subcellular Localization of Wild-Type and Parkinson's Disease-Associated Mutant α -Synuclein in Human and Transgenic Mouse Brain. *J. Neurosci.* **20**, 6365–6373 (2000).
86. Sharon, R. *et al.* α -Synuclein occurs in lipid-rich high molecular weight complexes, binds fatty acids, and shows homology to the fatty acid-binding proteins. *Proc. Natl. Acad. Sci.* **98**, 9110–9115 (2001).
87. Luäcke, C., Gantz, D. L., Klimtchuk, E. & Hamilton, J. A. Interactions between fatty acids and α -synuclein. *J. Lipid Res.* **47**, 1714–1724 (2006).
88. Ostrerova, N. *et al.* α -Synuclein Shares Physical and Functional Homology with 14-3-3 Proteins. *J. Neurosci.* **19**, 5782–5791 (1999).
89. Scott, D. & Roy, S. α -Synuclein Inhibits Intersynaptic Vesicle Mobility and Maintains Recycling-Pool Homeostasis. *J. Neurosci.* **32**, 10129–10135 (2012).
90. Chandra, S., Chen, X., Rizo, J., Jahn, R. & Südhof, T. C. A Broken α -Helix in Folded α -Synuclein. *J. Biol. Chem.* **278**, 15313–15318 (2003).
91. Bendor, J. T., Logan, T. P. & Edwards, R. H. The Function of α -Synuclein. *Neuron* **79**, 1044–1066 (2013).
92. Spillantini, M. G. *et al.* α -Synuclein in Lewy bodies. *Nature* **388**, 839–840 (1997).
93. Peng, C., Gathagan, R. J. & Lee, V. M.-Y. Distinct α -Synuclein strains and implications for heterogeneity among α -Synucleinopathies. *Neurobiol. Dis.* **109**, 209–218 (2018).

94. Guo, J. L. *et al.* Distinct α -Synuclein Strains Differentially Promote Tau Inclusions in Neurons. *Cell* **154**, 103–117 (2013).
95. Bousset, L. *et al.* Structural and functional characterization of two alpha-synuclein strains. *Nat. Commun.* **4**, 2575 (2013).
96. Peelaerts, W. *et al.* α -Synuclein strains cause distinct synucleinopathies after local and systemic administration. *Nature* **522**, 340–344 (2015).
97. Kim, C. *et al.* Exposure to bacterial endotoxin generates a distinct strain of α -synuclein fibril. *Sci. Rep.* **6**, 30891 (2016).
98. Lau, A. *et al.* α -Synuclein strains target distinct brain regions and cell types. *Nat. Neurosci.* **23**, 21–31 (2020).
99. Prusiner, S. B. *et al.* Evidence for α -synuclein prions causing multiple system atrophy in humans with parkinsonism. *Proc. Natl. Acad. Sci.* **112**, (2015).
100. Yamasaki, T. R. *et al.* Parkinson's disease and multiple system atrophy have distinct α -synuclein seed characteristics. *J. Biol. Chem.* **18**, 1045–1058 (2019).
101. Woerman, A. L. *et al.* Propagation of prions causing synucleinopathies in cultured cells. *Proc. Natl. Acad. Sci.* **112**, (2015).
102. Peng, C. *et al.* Cellular milieu imparts distinct pathological α -synuclein strains in α -synucleinopathies. *Nature* **557**, 558–563 (2018).
103. Strohäker, T. *et al.* Structural heterogeneity of α -synuclein fibrils amplified from patient brain extracts. *Nat. Commun.* **10**, 5535 (2019).
104. Schweighauser, M. *et al.* Structures of α -synuclein filaments from multiple system atrophy. *Nature* **585**, 464–469 (2020).
105. Savica, R., Grossardt, B. R., Bower, J. H., Ahlskog, J. E. & Rocca, W. A. Time Trends in the Incidence of Parkinson Disease. *JAMA Neurol.* **73**, 981 (2016).
106. Postuma, R. B. *et al.* MDS clinical diagnostic criteria for Parkinson's disease: MDS-PD Clinical Diagnostic Criteria. *Mov. Disord.* **30**, 1591–1601 (2015).

107. Kaufmann, H. *et al.* Natural history of pure autonomic failure: A United States prospective cohort: Pure Autonomic Failure. *Ann. Neurol.* **81**, 287–297 (2017).
108. Högl, B., Stefani, A. & Videnovic, A. Idiopathic REM sleep behaviour disorder and neurodegeneration — an update. *Nat. Rev. Neurol.* **14**, 40–55 (2018).
109. Aarsland, D., Andersen, K., Larsen, J. P. & Lolk, A. Prevalence and Characteristics of Dementia in Parkinson Disease: An 8-Year Prospective Study. *Arch. Neurol.* **60**, 387 (2003).
110. Levy, G. *et al.* Combined effect of age and severity on the risk of dementia in Parkinson's disease. *Ann. Neurol.* **51**, 722–729 (2002).
111. Hely, M. A., Reid, W. G. J., Adena, M. A., Halliday, G. M. & Morris, J. G. L. The Sydney multicenter study of Parkinson's disease: The inevitability of dementia at 20 years: Twenty Year Sydney Parkinson's Study. *Mov. Disord.* **23**, 837–844 (2008).
112. Walker, Z., Possin, K. L., Boeve, B. F. & Aarsland, D. Lewy body dementias. *The Lancet* **386**, 1683–1697 (2015).
113. Savica, R. *et al.* Incidence of Dementia With Lewy Bodies and Parkinson Disease Dementia. *JAMA Neurol.* **70**, 1396 (2013).
114. Vann Jones, S. A. & O'Brien, J. T. The prevalence and incidence of dementia with Lewy bodies: a systematic review of population and clinical studies. *Psychol. Med.* **44**, 673–683 (2014).
115. Donaghy, P. C. *et al.* Neuropsychiatric symptoms and cognitive profile in mild cognitive impairment with Lewy bodies. *Psychol. Med.* **48**, 2384–2390 (2018).
116. McKeith, I. G. *et al.* Diagnosis and management of dementia with Lewy bodies: Fourth consensus report of the DLB Consortium. *Neurology* **89**, 88–100 (2017).
117. Ferman, T. J. *et al.* Nonamnesic mild cognitive impairment progresses to dementia with Lewy bodies. *Neurology* **81**, 2032–2038 (2013).
118. McKeith, I. G. *et al.* Research criteria for the diagnosis of prodromal dementia with Lewy bodies. *Neurology* **28**, 743–755 (2020).

119. Iranzo, A., Santamaria, J. & Tolosa, E. Idiopathic rapid eye movement sleep behaviour disorder: diagnosis, management, and the need for neuroprotective interventions. *Lancet Neurol.* **15**, 405–419 (2016).
120. Claassen, D. O. *et al.* REM sleep behavior disorder preceding other aspects of synucleinopathies by up to half a century. *Neurology* **75**, 494–499 (2010).
121. Iranzo, A. *et al.* Neurodegenerative disease status and post-mortem pathology in idiopathic rapid-eye-movement sleep behaviour disorder: an observational cohort study. *Lancet Neurol.* **12**, 443–453 (2013).
122. Postuma, R. B., Iranzo, A., Hu, M. T. M. & Pelletier, A. Risk and predictors of dementia and parkinsonism in idiopathic REM sleep behaviour disorder: a multicentre study. *Brain* **1;142**, 744–759 (2019).
123. Kordower, J. H., Chu, Y., Hauser, R. A., Freeman, T. B. & Olanow, C. W. Lewy body-like pathology in long-term embryonic nigral transplants in Parkinson's disease. *Nat. Med.* **14**, 504–506 (2008).
124. Li, J.-Y. *et al.* Lewy bodies in grafted neurons in subjects with Parkinson's disease suggest host-to-graft disease propagation. *Nat. Med.* **14**, 501–503 (2008).
125. Jan, A., Gonçalves, N. P., Vaegter, C. B., Jensen, P. H. & Ferreira, N. The Prion-Like Spreading of Alpha-Synuclein in Parkinson's Disease: Update on Models and Hypotheses. *Int. J. Mol. Sci.* **22**, 8338 (2021).
126. Kordower, J. H. *et al.* Transfer of host-derived alpha synuclein to grafted dopaminergic neurons in rat. *Neurobiol. Dis.* **43**, 552–557 (2011).
127. Mougnot, A.-L. *et al.* Prion-like acceleration of a synucleinopathy in a transgenic mouse model. *Neurobiol. Aging* **33**, 2225–2228 (2012).
128. Luk, K. C. *et al.* Pathological α -Synuclein Transmission Initiates Parkinson-like Neurodegeneration in Nontransgenic Mice. *Science* **338**, 949–953 (2012).

129. Masuda-Suzukake, M. *et al.* Prion-like spreading of pathological α -synuclein in brain. *Brain* **136**, 1128–1138 (2013).
130. Volpicelli-Daley, L. A. *et al.* Exogenous α -Synuclein Fibrils Induce Lewy Body Pathology Leading to Synaptic Dysfunction and Neuron Death. *Neuron* **72**, 57–71 (2011).
131. Lee, H.-J. Intravesicular Localization and Exocytosis of α -Synuclein and its Aggregates. *J. Neurosci.* **25**, 6016–6024 (2005).
132. Emmanouilidou, E. *et al.* Cell-Produced α -Synuclein Is Secreted in a Calcium-Dependent Manner by Exosomes and Impacts Neuronal Survival. *J. Neurosci.* **30**, 6838–6851 (2010).
133. Jang, A. *et al.* Non-classical exocytosis of α -synuclein is sensitive to folding states and promoted under stress conditions. *J. Neurochem.* (2010) doi:10.1111/j.1471-4159.2010.06695.x.
134. Uemura, N., Uemura, M. T., Luk, K. C., Lee, V. M.-Y. & Trojanowski, J. Q. Cell-to-Cell Transmission of Tau and α -Synuclein. *Trends Mol. Med.* **26**, 936–952 (2020).
135. Peng, C., Trojanowski, J. Q. & Lee, V. M.-Y. Protein transmission in neurodegenerative disease. *Nat. Rev. Neurol.* **16**, 199–212 (2020).
136. Fares, M. B., Jagannath, S. & Lashuel, H. A. Publisher Correction: Reverse engineering Lewy bodies: how far have we come and how far can we go? *Nat. Rev. Neurosci.* **22**, 256–256 (2021).
137. Zhang, S. *et al.* Mechanistic basis for receptor-mediated pathological α -synuclein fibril cell-to-cell transmission in Parkinson's disease. *Proc. Natl. Acad. Sci.* **118**, e2011196118 (2021).
138. Mao, X. *et al.* Pathological α -synuclein transmission initiated by binding lymphocyte-activation gene 3. *Science* **353**, aah3374 (2016).
139. Reyes, J. F. *et al.* Alpha-synuclein transfers from neurons to oligodendrocytes. *Glia* **62**, 387–398 (2014).

140. Braak, H., Rüb, U., Gai, W. P. & Del Tredici, K. Idiopathic Parkinson's disease: possible routes by which vulnerable neuronal types may be subject to neuroinvasion by an unknown pathogen. *J. Neural Transm.* **110**, 517–536 (2003).
141. Stokholm, M. G., Danielsen, E. H., Hamilton-Dutoit, S. J. & Borghammer, P. Pathological α -synuclein in gastrointestinal tissues from prodromal Parkinson disease patients: α -Synuclein in Prodromal PD. *Ann. Neurol.* **79**, 940–949 (2016).
142. Hilton, D. *et al.* Accumulation of α -synuclein in the bowel of patients in the pre-clinical phase of Parkinson's disease. *Acta Neuropathol. (Berl.)* **127**, 235–241 (2014).
143. Breid, S. *et al.* Neuroinvasion of α -Synuclein Prionoids after Intraperitoneal and Intraglossal Inoculation. *J. Virol.* **90**, 9182–9193 (2016).
144. Ayers, J. I. *et al.* Robust Central Nervous System Pathology in Transgenic Mice following Peripheral Injection of α -Synuclein Fibrils. *J. Virol.* **91**, e02095-16 (2017).
145. Kocisko, D. A. *et al.* Cell-free formation of protease-resistant prion protein. *Nature* **370**, 471–474 (1994).
146. Barria, M. A., Mukherjee, A., Gonzalez-Romero, D., Morales, R. & Soto, C. De Novo Generation of Infectious Prions In Vitro Produces a New Disease Phenotype. *PLoS Pathog.* **5**, e1000421 (2009).
147. Soto, C. *et al.* Pre-symptomatic detection of prions by cyclic amplification of protein misfolding. *FEBS Lett.* **579**, 638–642 (2005).
148. Cosseddu, G. M. *et al.* Ultra-Efficient PrPSc Amplification Highlights Potentialities and Pitfalls of PMCA Technology. *PLoS Pathog.* **7**, e1002370 (2011).
149. Atarashi, R. *et al.* Ultrasensitive detection of scrapie prion protein using seeded conversion of recombinant prion protein. *Nat. Methods* **4**, 645–650 (2007).
150. Colby, D. W. *et al.* Prion detection by an amyloid seeding assay. *Proc. Natl. Acad. Sci.* **104**, 20914–20919 (2007).

151. Wilham, J. M. *et al.* Rapid End-Point Quantitation of Prion Seeding Activity with Sensitivity Comparable to Bioassays. *PLoS Pathog.* **6**, e1001217 (2010).
152. Ferreira, N. C. *et al.* Detection of chronic wasting disease in mule and white-tailed deer by RT-QuIC analysis of outer ear. *Sci. Rep.* **11**, 7702 (2021).
153. Atarashi, R. *et al.* Ultrasensitive human prion detection in cerebrospinal fluid by real-time quaking-induced conversion. *Nat. Med.* **17**, 175–178 (2011).
154. Orrú, C. D. *et al.* A Test for Creutzfeldt–Jakob Disease Using Nasal Brushings. *N. Engl. J. Med.* **371**, 519–529 (2014).
155. Lattanzio, F. *et al.* Prion-specific and surrogate CSF biomarkers in Creutzfeldt–Jakob disease: diagnostic accuracy in relation to molecular subtypes and analysis of neuropathological correlates of p-tau and A β 42 levels. *Acta Neuropathol. (Berl.)* **133**, 559–578 (2017).
156. Franceschini, A. *et al.* High diagnostic value of second generation CSF RT-QuIC across the wide spectrum of CJD prions. *Sci. Rep.* **7**, 10655 (2017).
157. Candelise, N., Baiardi, S., Franceschini, A., Rossi, M. & Parchi, P. Towards an improved early diagnosis of neurodegenerative diseases: the emerging role of in vitro conversion assays for protein amyloids. *Acta Neuropathol. Commun.* **8**, 117 (2020).
158. Poleggi, A., Baiardi, S., Ladogana, A. & Parchi, P. The Use of Real-Time Quaking-Induced Conversion for the Diagnosis of Human Prion Diseases. *Front. Aging Neurosci.* **14**, 874734 (2022).
159. Simrén, J., Ashton, N. J., Blennow, K. & Zetterberg, H. An update on fluid biomarkers for neurodegenerative diseases: recent success and challenges ahead. *Curr. Opin. Neurobiol.* **61**, 29–39 (2020).
160. Ayers, J. I., Paras, N. A. & Prusiner, S. B. Expanding spectrum of prion diseases. *Emerg. Top. Life Sci.* **4**, 155–167 (2020).
161. Abu-Rumeileh, S. *et al.* Diagnostic value of surrogate CSF biomarkers for Creutzfeldt–Jakob disease in the era of RT-QuIC. *J. Neurol.* **266**, 3136–3143 (2019).

162. Baiardi, S., Capellari, S., Bartoletti Stella, A. & Parchi, P. Unusual Clinical Presentations Challenging the Early Clinical Diagnosis of Creutzfeldt-Jakob Disease. *J. Alzheimers Dis.* **64**, 1051–1065 (2018).
163. Bongianni, M. *et al.* Diagnosis of Human Prion Disease Using Real-Time Quaking-Induced Conversion Testing of Olfactory Mucosa and Cerebrospinal Fluid Samples. *JAMA Neurol.* **74**, 155 (2017).
164. McGuire, L. I. *et al.* Real time quaking-induced conversion analysis of cerebrospinal fluid in sporadic Creutzfeldt-Jakob disease. *Ann. Neurol.* **72**, 278–285 (2012).
165. Sano, K. *et al.* Early Detection of Abnormal Prion Protein in Genetic Human Prion Diseases Now Possible Using Real-Time QuIC Assay. *PLoS ONE* **8**, e54915 (2013).
166. Cramm, M. *et al.* Stability and Reproducibility Underscore Utility of RT-QuIC for Diagnosis of Creutzfeldt-Jakob Disease. *Mol. Neurobiol.* **53**, 1896–1904 (2016).
167. McGuire, L. I. *et al.* Cerebrospinal fluid real-time quaking-induced conversion is a robust and reliable test for sporadic creutzfeldt-jakob disease: An international study: sCJD CSF RT-QuIC. *Ann. Neurol.* **80**, 160–165 (2016).
168. Cramm, M. *et al.* Characteristic CSF Prion Seeding Efficiency in Humans with Prion Diseases. *Mol. Neurobiol.* **51**, 396–405 (2015).
169. Orrú, C. D. *et al.* Bank Vole Prion Protein As an Apparently Universal Substrate for RT-QuIC-Based Detection and Discrimination of Prion Strains. *PLOS Pathog.* **11**, e1004983 (2015).
170. Mok, T. H. *et al.* Bank vole prion protein extends the use of RT-QuIC assays to detect prions in a range of inherited prion diseases. *Sci. Rep.* **11**, 5231 (2021).
171. Orrú, C. D. *et al.* Rapid and Sensitive RT-QuIC Detection of Human Creutzfeldt-Jakob Disease Using Cerebrospinal Fluid. *mBio* **6**, e02451-14 (2015).
172. Groveman, B. R. *et al.* Extended and direct evaluation of RT-QuIC assays for Creutzfeldt-Jakob disease diagnosis. *Ann. Clin. Transl. Neurol.* **4**, 139–144 (2017).

173. Högl, B., Stefani, A. & Videnovic, A. Idiopathic REM sleep behaviour disorder and neurodegeneration — an update. *Nat. Rev. Neurol.* **14**, 40–55 (2018).
174. Kaufmann, H. *et al.* Natural history of pure autonomic failure: A United States prospective cohort: Pure Autonomic Failure. *Ann. Neurol.* **81**, 287–297 (2017).
175. Miki, Y. *et al.* Improving diagnostic accuracy of multiple system atrophy: a clinicopathological study. *Brain* **142**, 2813–2827 (2019).
176. Postuma, R. B. *et al.* Validation of the MDS clinical diagnostic criteria for Parkinson’s disease: Validation of MDS Criteria. *Mov. Disord.* **33**, 1601–1608 (2018).
177. Koga, S. & Dickson, D. W. Recent advances in neuropathology, biomarkers and therapeutic approach of multiple system atrophy. *J. Neurol. Neurosurg. Psychiatry* **89**, 175–184 (2018).
178. Fairfoul, G. *et al.* Alpha-synuclein RT -Qu IC in the CSF of patients with alpha-synucleinopathies. *Ann. Clin. Transl. Neurol.* **3**, 812–818 (2016).
179. Shahnawaz, M. *et al.* Development of a Biochemical Diagnosis of Parkinson Disease by Detection of α -Synuclein Misfolded Aggregates in Cerebrospinal Fluid. *JAMA Neurol.* **74**, 163 (2017).
180. Groveman, B. R. *et al.* Rapid and ultra-sensitive quantitation of disease-associated α -synuclein seeds in brain and cerebrospinal fluid by α Syn RT-QuIC. *Acta Neuropathol. Commun.* **6**, 7 (2018).
181. Rossi, M. *et al.* Ultrasensitive RT-QuIC assay with high sensitivity and specificity for Lewy body-associated synucleinopathies. *Acta Neuropathol. (Berl.)* **140**, 49–62 (2020).
182. Head, M. W. *et al.* Prion Protein Accumulation in Eyes of Patients with Sporadic and Variant Creutzfeldt-Jakob Disease. *Investig. Ophthalmology Vis. Sci.* **44**, 342 (2003).
183. Zanusso, G. *et al.* Detection of Pathologic Prion Protein in the Olfactory Epithelium in Sporadic Creutzfeldt–Jakob Disease. *N. Engl. J. Med.* **348**, 711–719 (2003).
184. Favereaux, A. *et al.* Pathologic Prion Protein Spreading in the Peripheral Nervous System of a Patient With Sporadic Creutzfeldt-Jakob Disease. *Arch. Neurol.* **61**, 747 (2004).

185. Orrù, C. D. *et al.* Prion seeding activity and infectivity in skin samples from patients with sporadic Creutzfeldt-Jakob disease. *Sci. Transl. Med.* **9**, eaam7785 (2017).
186. Baiardi, S. *et al.* Prion-related peripheral neuropathy in sporadic Creutzfeldt-Jakob disease. *J. Neurol. Neurosurg. Psychiatry* **90**, 424–427 (2019).
187. Glatzel, M., Abela, E., Maissen, M. & Aguzzi, A. Extraneural Pathologic Prion Protein in Sporadic Creutzfeldt–Jakob Disease. *N. Engl. J. Med.* **349**, 1812–1820 (2003).
188. Fiorini, M. *et al.* High Diagnostic Accuracy of RT-QuIC Assay in a Prospective Study of Patients with Suspected sCJD. *Int. J. Mol. Sci.* **21**, 880 (2020).
189. Orrù, C. D. *et al.* Prion Seeds Distribute throughout the Eyes of Sporadic Creutzfeldt-Jakob Disease Patients. *mBio* **9**, e02095-18 (2018).
190. Wang, Z. *et al.* Early preclinical detection of prions in the skin of prion-infected animals. *Nat. Commun.* **10**, 247 (2019).
191. Bongianni, M. *et al.* Olfactory swab sampling optimization for α -synuclein aggregate detection in patients with Parkinson’s disease. *Transl. Neurodegener.* **11**, 37 (2022).
192. Perra, D. *et al.* Alpha-synuclein seeds in olfactory mucosa and cerebrospinal fluid of patients with dementia with Lewy bodies. *Brain Commun.* **3**, fcab045 (2021).
193. De Luca, C. M. G. *et al.* Efficient RT-QuIC seeding activity for α -synuclein in olfactory mucosa samples of patients with Parkinson’s disease and multiple system atrophy. *Transl. Neurodegener.* **8**, 24 (2019).
194. Wang, Z. *et al.* Skin α -Synuclein Aggregation Seeding Activity as a Novel Biomarker for Parkinson Disease. *JAMA Neurol.* **78**, 30 (2021).
195. Manne, S. *et al.* Blinded RT-QuIC Analysis of α -Synuclein Biomarker in Skin Tissue From Parkinson’s Disease Patients. *Mov. Disord.* **35**, 2230–2239 (2020).
196. Luan, M. *et al.* Diagnostic Value of Salivary Real-Time Quaking-Induced Conversion in Parkinson’s Disease and Multiple System Atrophy. *Mov. Disord.* **37**, 1059–1063 (2022).

197. Shin, C. *et al.* In vivo and autopsy validation of alpha-synuclein seeding activity using RT-QuIC assay in the gastrointestinal tract of patients with Parkinson's disease. *Parkinsonism Relat. Disord.* **103**, 23–28 (2022).
198. De Luca, C. M. G. *et al.* Efficient RT-QuIC seeding activity for α -synuclein in olfactory mucosa samples of patients with Parkinson's disease and multiple system atrophy. *Transl. Neurodegener.* **8**, 24 (2019).
199. Mammana, A. *et al.* Detection of prions in skin punch biopsies of Creutzfeldt–Jakob disease patients. *Ann. Clin. Transl. Neurol.* **7**, 559–564 (2020).
200. Mammana, A. *et al.* RT-QuIC Detection of Pathological α -Synuclein in Skin Punches of Patients with Lewy Body Disease. *Mov. Disord.* **36**, 2173–2177 (2021).
201. Parchi, P. *et al.* Incidence and spectrum of sporadic Creutzfeldt–Jakob disease variants with mixed phenotype and co-occurrence of PrPSc types: an updated classification. *Acta Neuropathol. (Berl.)* **118**, 659–671 (2009).
202. Parchi, P. *et al.* Consensus classification of human prion disease histotypes allows reliable identification of molecular subtypes: an inter-rater study among surveillance centres in Europe and USA. *Acta Neuropathol. (Berl.)* **124**, 517–529 (2012).
203. Montine, T. J. *et al.* National Institute on Aging–Alzheimer's Association guidelines for the neuropathologic assessment of Alzheimer's disease: a practical approach. *Acta Neuropathol. (Berl.)* **123**, 1–11 (2012).
204. Alafuzoff, I. *et al.* Staging/typing of Lewy body related α -synuclein pathology: a study of the BrainNet Europe Consortium. *Acta Neuropathol. (Berl.)* **117**, 635–652 (2009).
205. Alafuzoff, I. *et al.* Staging of Neurofibrillary Pathology in Alzheimer's Disease: A Study of the BrainNet Europe Consortium. *Brain Pathol.* **0**, 080509082911413-??? (2008).
206. Zerr, I. *et al.* Updated clinical diagnostic criteria for sporadic Creutzfeldt-Jakob disease. *Brain* **132**, 2659–2668 (2009).

207. Donadio, V. *et al.* Skin nerve α -synuclein deposits: A biomarker for idiopathic Parkinson disease. *Neurology* **82**, 1362–1369 (2014).
208. Lauria, G. *et al.* European Federation of Neurological Societies/Peripheral Nerve Society Guideline on the use of skin biopsy in the diagnosis of small fiber neuropathy. Report of a joint task force of the European Federation of Neurological Societies and the Peripheral Nerve Society. *Eur. J. Neurol.* **17**, 903–e49 (2010).
209. Orrù, C. D. *et al.* RT-QuIC Assays for Prion Disease Detection and Diagnostics. in *Prions* (ed. Lawson, V. A.) vol. 1658 185–203 (Springer New York, 2017).
210. Orrù, C. D. *et al.* A rapid α -synuclein seed assay of Parkinson's disease CSF panel shows high diagnostic accuracy. *Ann. Clin. Transl. Neurol.* **8**, 374–384 (2021).
211. Donadio, V. Skin nerve α -synuclein deposits in Parkinson's disease and other synucleinopathies: a review. *Clin. Auton. Res.* **29**, 577–585 (2019).
212. Iranzo, A. *et al.* Detection of α -synuclein in CSF by RT-QuIC in patients with isolated rapid-eye-movement sleep behaviour disorder: a longitudinal observational study. *Lancet Neurol.* **20**, 203–212 (2021).
213. Yoo, D. *et al.* Diagnostic value of α -synuclein seeding amplification assays in α -synucleinopathies: A systematic review and meta-analysis. *Parkinsonism Relat. Disord.* S1353802022003261 (2022) doi:10.1016/j.parkreldis.2022.10.007.
214. Stefani, A. *et al.* Alpha-synuclein seeds in olfactory mucosa of patients with isolated REM sleep behaviour disorder. *Brain* **144**, 1118–1126 (2021).